HOLOGRAPHIC INTERFEROMETRY AND ITS APPLICATION TO VISUALISATION OF LARGE DEFORMATIONS AND OBTAINING RELIEF HOLOGRAMS ON AGFA 8E56HD EMULSION

A THESIS SUBMITTED TO
THE GRADUATE SCHOOL OF NATURAL AND APPLIED SCIENCES
OF
THE MIDDLE EAST TECHNICAL UNIVERSITY

BY

FEVZİ NECATİ ECEVİT

IN PARTIAL FULFILMENT OF THE REQUIREMENTS FOR THE DEGREE
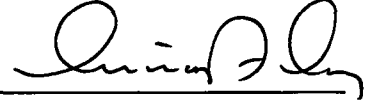OF

DOCTOR OF PHILOSOPHY

IN

THE DEPARTMENT OF PHYSICS

SEPTEMBER 1995

Approval of the Graduate School of Natural and Applied Sciences
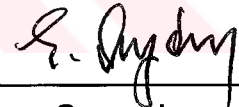
Prof. Dr. İsmail Tosun

for Director

I certify that this thesis satisfies all the requirements as a thesis for the degree of Doctor of Philosophy.

Prof. Dr. Mehmet Tomak

Head of Department

We certify that we have read this thesis and that in our opinion it is fully adequate, in scope and quality, as a thesis for the degree of Doctor of Philosophy.
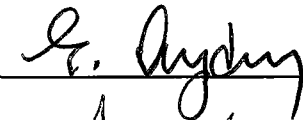
Prof. Dr. Ramazan Aydın

Supervisor

Examining Committee Members

Prof. Dr. Ediz Paykoç (chairman)

Prof. Dr. Ramazan Aydın

Prof. Dr. Hüseyin Akçay

Prof. Dr. Nizami Gassanly

Assoc. Prof. Dr. Tuncay İncesu

ABSTRACT

HOLOGRAPHIC INTERFEROMETRY AND ITS APPLICATION TO VISUALISATION OF LARGE DEFORMATIONS AND OBTAINING RELIEF HOLOGRAMS ON AGFA 8E56HD EMULSION

Ecevit, Fevzi Necati
Ph.D., Department of Physics
Supervisor: Prof. Dr. Ramazan Aydın

September 1995, 106 pages

Holographic interferometry has found an extensive use in the measurement of displacements, strains of rough objects and changes of refractive index due to some external effects.

In order to visualise these changes on different objects, different methods of holographic interferometry, double-exposure, difference holographic interferometry, are implemented in our laboratory. The double exposure method is used to visualise the refractive index changes in a lamp due to the heating of the filament and visualise the displacements caused by some mechanical and heating effects. For the comparison of displacements of two similar but different objects under the same loading conditions, the difference holographic interferometry method is used to visualise the difference of displacements.

To obtain relief holograms on Agfa 8E56 HD photographic emulsion, a chemical processing method is applied and their profile shapes are imaged by an atomic force microscope (AFM). The effect of exposure and spatial frequency on the relief shape of grating holograms are presented.

ÖZ

HOLOGRAFİK İNTERFEROMETRİ VE BÜYÜK DEFORMASYONLARIN GÖZLENMESİNE UYGULAMASI VE AGFA 8E56HD EMÜLSİYONU ÜZERİNDE RÖLYEF HOLOGRAM OLUŞTURULMASI

Ecevit, Fevzi Necati
Doktora, Fizik Bölümü
Tez Yöneticisi: Prof. Dr. Ramazan Aydın

Eylül 1995, 106 sayfa

Holografik interferometri cisimlerdeki yerdeğiştirmelerin, gerilme dağılımının ve kırınma indeks'lerindeki değişmelerin ölçülmesinde çok geniş bir şekilde kullanılmaktadır.

Bu değişiklikleri çeşitli cisimler üzerinde gözlemek amacıyla, holografik interferometrenin çeşitli yöntemleri, çift - çekim ve fark holografik interferometri teknikleri kullanılarak laboratuvarımızda denendi ve test edildi. Çift-çekim tekniği ile bir ampülün içindeki ortamın uygulanan voltaj ile kırınma indeksindeki değişimi ve bazı cisimler üzerine mekanik kuvvet ve ısıtma uygulayarak üzerindeki yerdeğiştirmeler gözlendi. Farklı, fakat iki benzer cisim üzerindeki yerdeğiştirmelerin farklarını gözlemek için fark holografik interferometri tekniği kullanıldı.

Agfa 8E56 HD fotoğraf plakasında rölyef holagram elde etmek için bir kimyasal işlemden geçirildi ve bu rölyeflerin yapısı atomik kuvvet mikroskopu ile görüntülendi. Pozlandırma süresinin ve rölyeflerin uzaysal dağılımının rölyeflerin şekline olan etkisi gözlendi.

Anahtar Kelimeler: Holografi, Çift-çekim Holografi, Fark Holografi, İnterferometri, Rölyef Hologramlar

ACKNOWLEDGEMENTS

TABLE OF CONTENTS

LIST OF TABLES

TABLE

LIST OF FIGURES

CHAPTER I

INTRODUCTION

Holography is a technique for recording an optical wavefront. It therefore differs from photography in the following important respect: photography records the intensity of a wavefront , as a function of position in the plane of the photographic plate, but insensitive to the phase of wavefront. Accordingly, in conjunction with an appropriate optical system (i.e., a focusing lens), photography produces a two-dimensional image of the object as a projection on the photographic plate. Holography also records the position-dependent intensity of a wavefront, but retains phase information and is, therefore, a coherent optical process. The retained phase information allows the recorded wavefront to be reconstructed to yield three-dimensional images.

The foundation of holography was laid in 1948 by Dennis Gabor [1,2]. Gabor set himself the task of improving the principles of electronic microscopy. He proposed to record, apart from amplitude information, phase information of electron waves by the superposition of a coherent reference wave and to reconstruct the image of an object from a diffraction pattern created at the recording. However, this technique became a reality only 14 years later with the advent of the laser, which provided the needed source of intense, coherent, monochromatic light. In Gabor's historical demonstration of holographic imaging, a transparency consisting of opaque lines on a clear background was illuminated with a collimated beam of monochromatic light,

and interference pattern produced by the directly transmitted beam (the reference wave) and light scattered by the lines on the transparency was recorded on a photographic plate. When the hologram (a positive transparency made from this plate) was illuminated with the original collimated beam, it produced two diffracted waves, one reconstructing an image of the object in its original location, and other, with the same amplitude but opposite phase, forming a second, conjugate image. However, a major drawback was that the conjugate image, as well as scattered light from the directly transmitted beam, seriously degraded the reconstructed image.

In 1962, Leith and Upatnieks [3] used laser beams and simultaneously varied the directions of both the object and reference waves in order to avoid their overlapping. This technique used a separate reference wave incident on the holographic plate at an appreciable angle to the object wave. As a result, when the hologram was illuminated with the original reference beam, two reconstructed images were separated by large enough angles from the directly transmitted beam, and from each other, to ensure that they did not overlap. In 1963, Denisyuk [4] and van Heerden [5] independently proposed recording in a three-dimensional medium, resulting in production of thick holograms, which have subsequently gained importance in information storage, in white light reconstruction, and other applications.

About 1965, it was technically possible to cause holographically produced wavefields to interfere with other wavefields, holographically or non-holographically produced, which resulted in fringe pattern. The first contributions in the fields of holographic interferometry were made by Powell and Stetson [6], Burch [7], Brooks et al. [8], Haines and Hildebrand [9]. Over the next few years, a number of investigators concentrated their efforts on developing the conceptual foundations for holographic interferometry. These

investigators have, for the most part, attempted to analyse the formation and localisation of fringes in holographic interferometry. Mathematical expressions were derived to relate the holographic interference fringes to the displacements and deformations of diffusely reflecting object. A self contained treatment of the subject can be found in the works of Vest [10], and Ostrovsky et al. [11-12], Schumann et al. [13-14], Rastogi [15].

Most of investigations were concerned with the deformation and vibration analysis of opaque bodies, on the other hand, and the determination of changes of indices of refraction in fluids (phase objects), on the other hand. These studies later found applications also in photoelasticity. In the following years holography developed mainly along the path of improving its applications.

Holograms may be used in any of the following ways:

- to produce 3-D image of object,
- to produce wavefronts that may then be analysed by interferometry,
- to produce the effect of optical components used to record holograms, and hence to produce a holographic optical element (HOE),
- to produce security cards, etc.

Holographic interferometry has proven to be a powerful tool for measuring deformations and non-destructive testing. Deformations of an opaque rough surface or refractive index variations of transparent body are measured to an accuracy of better than the wavelength of the used laser light. The main advantages of this method are:

- the measurements are contactless and non-invasive,
- the measurements are made on rough, diffusely reflecting surfaces; no specular reflection is required,

- two dimensional continuous information are obtained,

- the surface may be of arbitrary shape,

- the areas of the examined surfaces range from a few mm^2 to m^2

- the measured displacements range roughly from 0.05 to 500μm

- reliable deformation analysis can be performed at low loading
intensities; the testing is non-destructive.

- the method is independent of the material properties; deformations of
hard or soft materials are measured; refractive-index variations in
 solids, fluids, gases, and even plasmas can be determined,

- the achievable resolution and accuracy of displacement measurement
allows subsequent numerical strain and stress calculations,

- the measurements can be made on moving surfaces,

- the measurements can be made in closed box-like structures like
pressure or vacuum chambers through transparent windows,

Holographic interferometry does not measure directly the inside
integrity of a specimen, like X-ray or ultrasonics, but records its behaviour
under an applied load. A defect in a structure may be critical with regard to a
loading type or loading direction but not to other. There are a number of
possible loading-types some of which are given below:

- direct mechanical loading: bending moment, tensile stress, torsional
stress, gravity,

- pressure loading: internal pressure in hollow vessels, pressure or
vacuum chambers,

- vibrational loading: acoustic fields by loudspeakers, electrodynamic
shakers in point contact,

- impulse loading: local impact,

- thermal loading: radiation sources, hot air jets, volatile fluids, high
power DC in conductive material.

For the use of holography in interferometry there are three distinct application areas:

1. The comparison of the wavefront from the object with a reference beam of known profile (such as plane wave) to produce an interferogram containing fringes that contour the object and hence describe its shape.

2. The comparison of wavefronts obtained from the object at different times to reveal changes in position of the object surface, thus allowing measurements of displacement, strain, and vibration.

3. The formation of interference fringes where the object beam has passed through a fluid or gas, thus revealing the changes in refractive index (related to temperature, pressure, density, or compositional changes), thus permitting flow visualisation or velocimetry.

Holographic interferometry has found an extensive use in experimental mechanics in the measurement of displacements and strains of rough objects. The method has been used with considerable amount of success in the non-destructive testing of materials and engineering components. The presence of flaws such as microcracks, voids, delaminations and material nonhomogeneities have all been unveiled by the method.

The most striking thing about holographic interferometry has been the sweep of its reach. From the inspection of aircraft components [16] to the study of crystal growth [17-20], from the bone structure studies[21-22] to the measurement of wear in prosthesis [23], from the evaluation of the frost resistance of porous materials [24-28] to the study of the mechanical behaviour of eardrum [29], from the studies of orthodontic tooth movements[30] to the measurements of flaws and cracks [31-32], from the

measurement of flows [33-35] to stress and strain analysis [36-37], from the measurement of thermal waves [38] to the measurements of distortion and deformation [39-42], from the measurement of corrosion [43], temperature [44] to the investigation of cutting tools [45], Poisson coefficient and elasticity moduli [46], inhomogeneity testing of glass [47] the applications of holographic interferometry have been far and wide touching upon fields as diverse as medicine, material testing, biology and environment.

Recent advances in digital image acquisition and processing technologies have been changing the nature of fringe pattern analysis towards an increasing reliance on computer based and optoelectronic approaches. The tedium and imprecision associated with mutual extraction of quantitative data from the interferograms has given way to the automatic evaluation of phase encoded in the fringe pattern. The high speed automatic reduction of fringe data not only provides a versatile service to practitioners but also, at the same time, makes the technique more economical and efficient to use.

Holography is a branch of optical interferometry, and practical requirements of that subject apply to it. Interferometry requires mechanical stability of optical components to within a fraction of an optical wavelength for the duration of the experiment and is also demanding in the quality of optical components used. But the development of high power and pulsed lasers has resulted in reduced exposure times, and hence the requirement for mechanical stability.

A second practical difficulty in holography is related to optical recording media used. The interferogram recorded by the holographic plate contains fine details, on the scale of optical wavelength. Traditionally, this high-resolution requirement has been met by wet chemical techniques.

These techniques are laborious and do not lend themselves to real-time applications or quantitative processing of the recorded data.

The second chapter is devoted mainly to the basic theory of off-axis holography and hologram types and intrinsic properties of holograms. In the third chapter, holographic interferometry and different techniques of holographic interferometry, mainly double-exposure and difference holographic interferometry techniques are discussed. The properties of light sources, optical elements, optoelectronic components used in holography and practical aspects of holography are explained in chapter 4. Holographic recording materials and their processing techniques are given in chapter 5. The experimental implementation of double-exposure, difference holographic interferometry and obtaining relief hologram structure results are presented in chapter 6.

CHAPTER II

BASIC THEORY OF HOLOGRAMS

In this section, basic theory of hologram formation, their reconstruction and types of holograms are discussed.

2.1 Basic Holography

A hologram is an interference pattern formed by an object wave and a reference wave [48]. The Figure 2.1 shows a set-up for preparing a hologram.
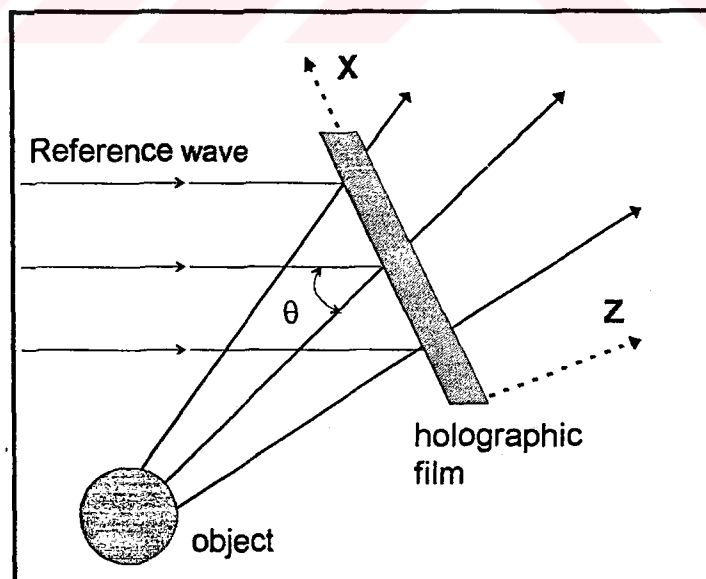
Figure 2.1. Hologram recording with an off-axis reference beam.

Light waves from an object and from a reference source fall on a photographic plate. By considering that the complex amplitude vectors of these waves are perpendicular to the plane of drawing, we can limit ourselves to a scalar treatment. The complex amplitudes of the object and reference waves in the plane of the hologram (x,y) can be written as

$$o(x,y) = |o(x,y)| exp(-i\phi_o(x,y))$$ (2.1)

while that due to the reference beam (plane wave) is

$$r(x,y) = r exp(i2\pi\xi_r x)$$ (2.2)

where $\xi_r = (sin\theta)/\lambda$, since the reference beam has uniform intensity and only its phase varies across the photographic plate . The resultant intensity at the photographic plate is

$$I(x,y) = |r(x,y) + o(x,y)|^2$$

$$= r^2 + |o(x,y)|^2 + 2r|o(x,y)|cos[2\pi\xi_r x + \phi(x,y)]$$ (2.3)

As can be seen from Eq.(2.3), the amplitude and phase of object wave are encoded, respectively, as amplitude and phase modulation of a set of interference fringes equivalent to a spatial carrier with a spatial frequency equal to ξ_r. If it is assumed that the amplitude transmittance of the photographic plate after processing is linearly related to the intensity in the interference pattern, the amplitude transmittance of the hologram can be written as

$$t(x,y) = t_o + \beta T\{|o(x,y)|^2 + r|o(x,y)|exp[-i(\phi(x,y) + 2\pi\xi_r x)]$$

$$+r|o(x,y)|exp[i(\phi(x,y) + 2\pi\xi_r x)]\}$$ (2.4)

9

where β is the slope of the amplitude transmittance versus exposure characteristic of the photographic material, T is the exposure time and t_0 is a constant background transmittance.

To reconstruct the image, the hologram is illuminated once again, as shown in Figure 2.2 with the same reference beam as was used to record it. The complex amplitude u(x,y) of the transmitted wave is the sum of four terms, each corresponding to one of the terms Eq.(2.4), and can be written as

$$u(x,y) = r(x,y)t(x,y),$$

$$= u_1(x,y) + u_2(x,y) + u_3(x,y) + u_4(x,y) \qquad (2.5)$$

where

$$u_1(x,y) = t_0 r \, exp(i2\pi\xi_r x) \qquad (2.6)$$

$$u_2(x,y) = \beta Tr|o(x,y)|^2 exp(i2\pi\xi_r x) \qquad (2.7)$$

$$u_3(x,y) = \beta Tr^2 o(x,y) \qquad (2.8)$$

$$u_4(x,y) = \beta Tr^2 o^*(x,y) exp(i4\pi\xi_r x) \qquad (2.9)$$

The first term on the right hand side of Eq.(2.5), $u_1(x,y)$, is merely the attenuated reference beam, which is a plane wave directly transmitted through the hologram. This directly transmitted beam is surrounded by a halo due to the second term, $u_2(x,y)$, which is spatially varying. The angular spread of this halo is determined by the angular extent of the object.
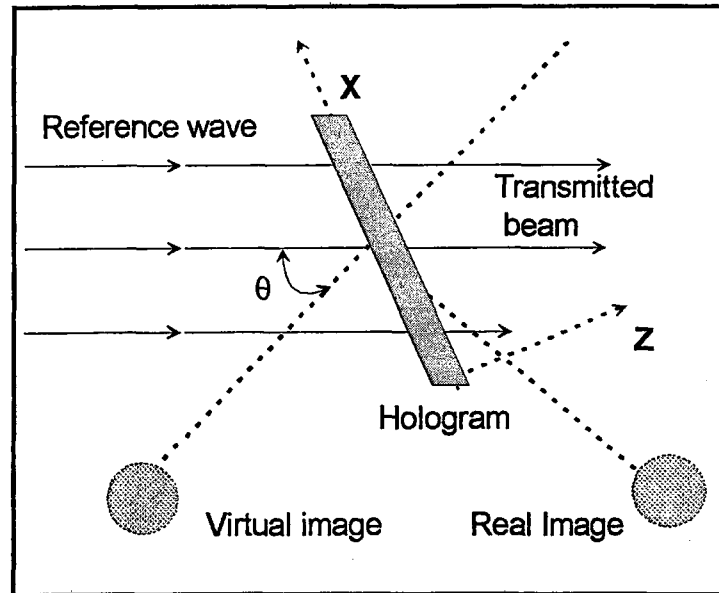
Figure 2.2. Hologram reconstruction

The third term, $u_3(x,y)$ is identical with the original object wave, except for a constant factor, and generates a virtual image of the object in its original position; this wave makes an angle θ with the directly transmitted wave. Similarly, the fourth term, $u_4(x,y)$, gives rise to the conjugate real image. However, fourth term includes an exponential factor, $exp(i4\pi\xi_x x)$, which indicates that the conjugate wave is deflected off the axis at an angle approximately twice that which the reference wave makes with it.

Thus, even though two images - one real and one virtual - are still reconstructed in this set-up, they are angularly separated from the transmitted beam and from each other, and if the offset angle of the reference beam is made large enough, it is possible to ensure that there is no overlap.

The minimum value of the offset angle θ required to ensure that each of the images can be observed without any interference from its twin, as well as from the directly transmitted beam and halo of scattered light

surrounding it, is determined by the spatial carrier frequency ξ_r for which there is no overlap between the angular spectra of the third and fourth terms and those of first and second terms. These angular spectra are the Fourier transforms of these terms and can be written as follows.

$$U_1(\xi,\eta) = F\{t_o r \, exp(i2\pi\xi_r x)\} = t_o r \delta(\xi+\xi_r,\eta) \tag{2.10}$$

$$U_2(\xi,\eta) = F\{\beta Tr|o(x,y)|^2 exp(i2\pi\xi_r x)\}$$
$$= \beta Tr[O(\xi,\eta) \oplus O(\xi,\eta)*\delta(\xi+\xi_r,\eta)] \tag{2.11}$$

where $O(\xi,\eta) = F\{o(x,y)\}$ is the spatial frequency spectrum of the object beam, and symbol $\oplus$ and $*$ denote, respectively, the operations of correlation and convolution.

$$U_3(\xi,\eta) = F\{\beta Tr^2 o(x,y)\} = \beta Tr^2 O(\xi,\eta) \tag{2,12}$$

$$U_4(\xi,\eta) = F\{\beta Tr^2 o^*(x,y) \, exp(i4\pi\xi_r x)\}$$
$$= \beta Tr^2 O(\xi,\eta)*\delta(\xi+2\xi_r,\eta) \tag{2.13}$$

As shown in Figure 2.3, which shows these spectra schematically, the term $|U_3|$ is merely the object beam spectrum multiplied by a constant and centred at the origin of the spatial frequency plane. The term $|U_1|$ corresponds to the spatial frequency of the carrier fringes and is a δ function located at $(-\xi_r,0)$, while $|U_2|$ is centred on this δ function and, being proportional to the auto-correlation function of $O(\xi,\eta)$, has twice the extent of the object beam spectrum. Finally, $|U_4|$ is similar to $|U_3|$ but is displaced to a centre frequency $(2\xi_r,0)$. Evidently, $|U_3|$ and $|U_4|$ will not overlap $|U_1|$ and $|U_2|$ if the spatial carrier frequency ξ is chosen so that
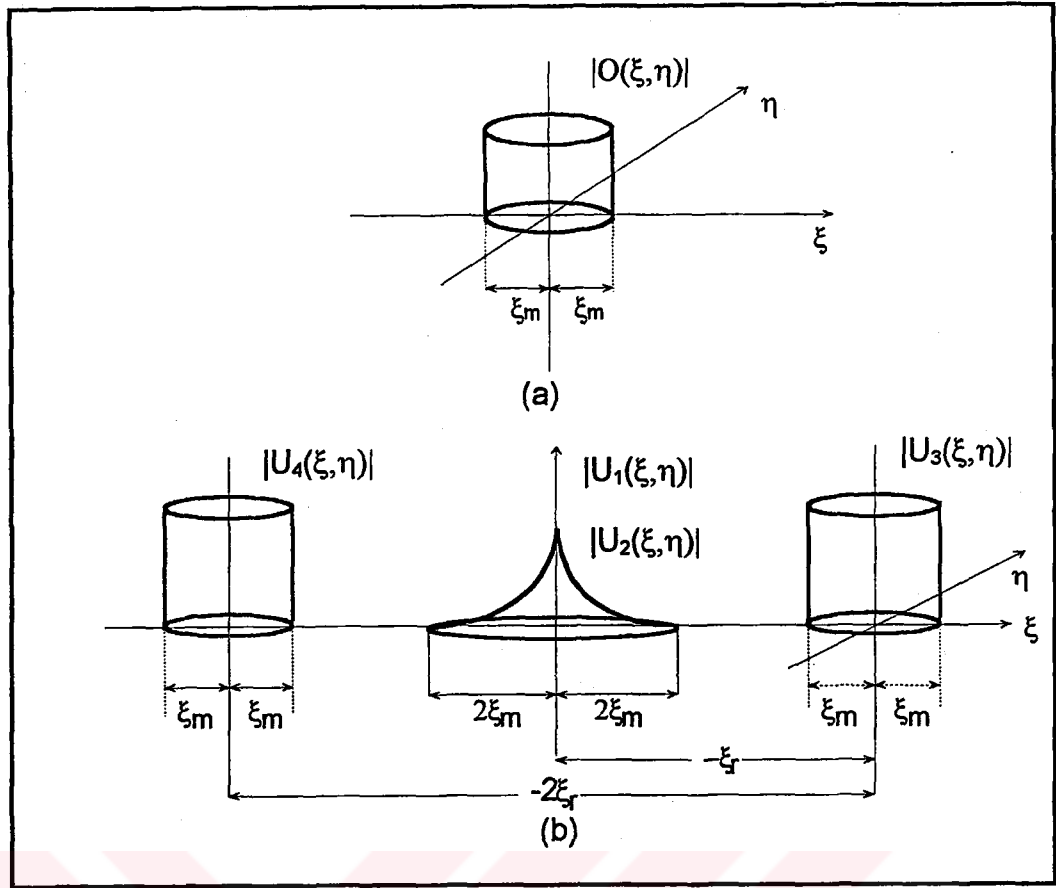
Figure 2.3. Spatial frequency spectra of (a) the object beam and (b) a hologram recorded with an off-axis reference beam.

$$\xi_r \geq 3\xi_m$$

where ξ_m is the highest frequency in the spatial frequency spectrum of the object beam.

2.2 Classification of Holograms

Holograms are classified as to type with the recording geometry, the type of modulation imposed on the illuminating wave, the thickness of the recording material, and the mode of image formation as factors [49].

If the two interfering beams are travelling in substantially the same direction, the recording of the interference pattern is said to be Gabor hologram or inline hologram. If the two interfering beams arrive at the recording medium from substantially directions, the recording is a Leith-Upatnieks or off-axis hologram. If the two interfering beams are travelling in essentially opposite directions, the recorded hologram is said to be Lippman or reflection hologram.

These hologram types are further classified, depending on recording geometry, as Fresnel, Fourier Transform, Fraunhofer, or Lensless Fourier Transform. Any of the foregoing hologram types also may be recorded as a thick or thin hologram. A thin (or plane) hologram is one for which the thickness of the recording medium is small compared to the fringe spacing. A thick (or volume) hologram is one for which the thickness of emulsion is of the order of or greater than the fringe spacing. The distinction between thick and thin holograms is usually made with the aid of the Q-parameter defined as

$$Q = \frac{2\pi\lambda d}{n\Lambda^2}$$

where λ is the illuminating wavelength, n the refractive index of the recording material, d its thickness, and Λ the spacing of the recorded fringes. The hologram is considered thick when $Q \geq 10$ and thin otherwise.

Finally, holograms are also classified by the mechanism by which the illuminating light is diffracted. In an amplitude hologram the interference pattern is recorded as a density variation of the recording medium, and amplitude of the illuminating wave is accordingly modulated. In a phase hologram, a phase modulation is imposed on the illuminating wave.

2.3 Reflection Holograms

If the object and reference beams are incident on the photographic plate from opposite sides, the interference fringes produced are actually layers within the thickness of the emulsion, about half a wavelength apart. A hologram recorded in this manner, illuminated with a point source of white light, can reconstruct a monochromatic image in reflected light. Simple recording and reconstruction geometries of the reflection holography are shown in Figure 2.4 and Figure 2.5.. The other types holograms can be found in references [48,50].
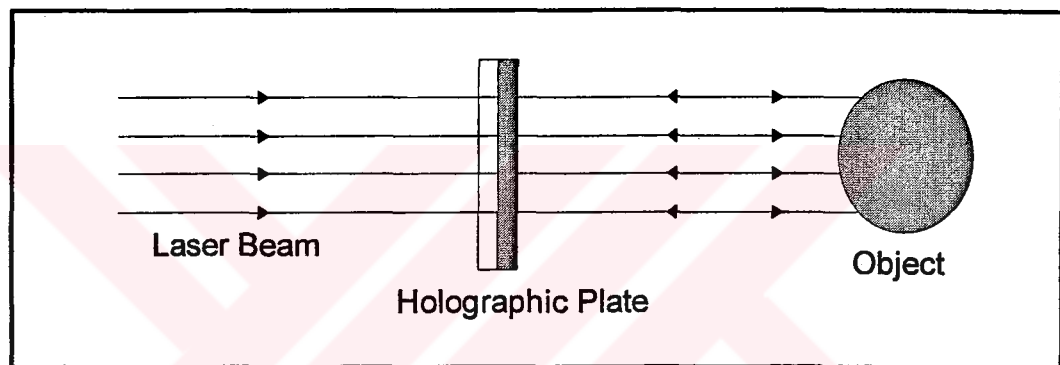
Figure 2.4. Recording a reflection hologram
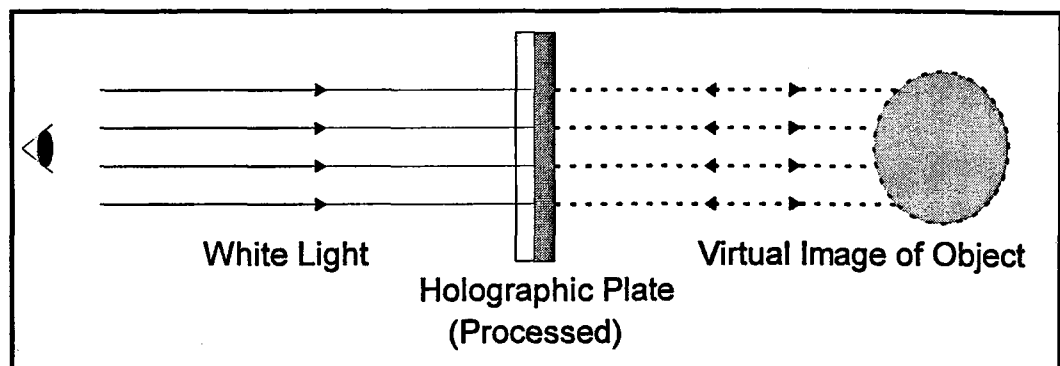
Figure 2.5. Reconstruction of a reflection hologram.

2.4 Macroscopic Characteristics of the Holographic Recording Process

The complex amplitude transmittance $T_a(x)$ of holographic recording material can be written in a general manner as

$$T_a = |t_a(x)| exp[-\alpha(x)d] exp[-i\phi_t(x)]$$
$$= |t_a(x)| exp[-\alpha(x)d] exp[-i2\pi nd / \lambda(x)] \qquad (2.15)$$

where α is the absorption constant of material, d the thickness, n the refractive index of the material, and λ the wavelength of the laser light. The amplitude transmittance T_a is the square root of the transmittance, $T_a = \sqrt{T}$.

There are two main types of holograms: amplitude and phase holograms. In a pure amplitude hologram ($\phi_t(x)$=const.) only the absorption α varies with the exposure (after processing), whereas in a pure phase hologram (α=0, $|t_a(x)|$=1) either n or d changes with exposure. For the phase hologram the phase factor is

$$\phi_t = \left(\frac{2\pi}{\lambda}\right)nd \qquad (2.16)$$

$$\Delta\phi_t = \left(\frac{2\pi}{\lambda}\right)[d\Delta n + (n-1)\Delta d] \qquad (2.17)$$

If the hologram is thin, $d \cong 0$: Phase variations are then caused by surface relief variations only

$$\Delta\phi_t = \left(\frac{2\pi}{\lambda}\right)(n-1)\Delta d \qquad (2.18)$$

16

If the hologram is thick and has a negligible surface relief ($\Delta d=0$), phase variations are caused by index variations only

$$\Delta\phi_t = \left(\frac{2\pi}{\lambda}\right)d\Delta n \qquad (2.19)$$

In many cases the phase modulation in a hologram is a combination of the two different extreme types (a complex hologram). For different types of recording materials and processing techniques one can obtain desired modulation mechanism. The detailed information on recording materials are given in chapter 5.

For amplitude holograms the amplitude transmission T_a against log exposure is used whereas for a phase hologram the corresponding curve is the phase shift against a log exposure relation, Figure 2.6, 2.7.
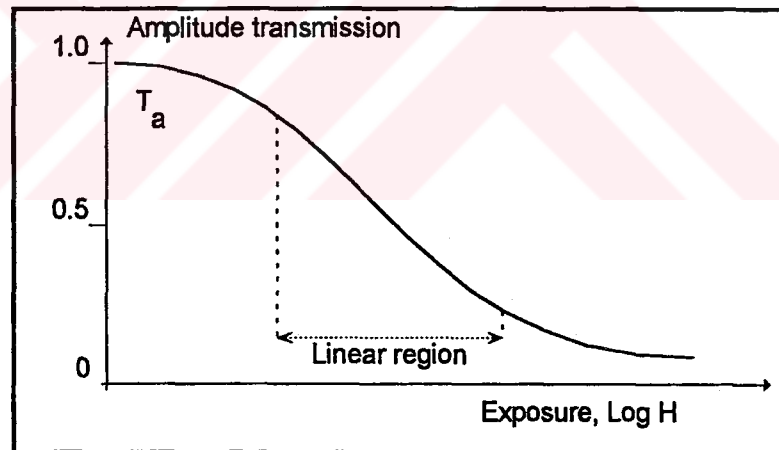
Figure 2.6. Amplitude transmission T_a versus the logarithm of exposure H used for the characterisation of amplitude transmission holograms.
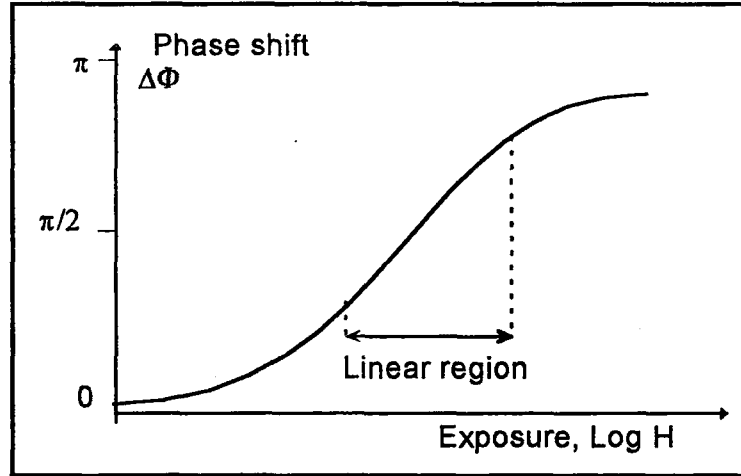
Figure 2.7. Phase shift Δφ versus the logarithm of exposure H used for the characterisation of phase transmission holograms.

2.5 Diffraction Efficiency

The recording material is exposed to intensity of the interference pattern during a certain time t. If the intensity distribution in the pattern is constant during the exposure, the total exposure of the material is

$$H=Et \qquad\qquad (2.20)$$

where E is the average intensity plus the intensity modulation (depending on the beam ratio, the phase, the original object intensity variations, and MTF of the material). If linear recording is assumed, these intensity variations will be recorded as density variations in the processed emulsion for an amplitude hologram. The density variations are causing an amplitude modulation of the reference beam, when the processed hologram is reconstructed. The amplitude modulation of the primary, first-order diffraction light is mainly of interest, since it contains the original scattered wavefront from the recorded object. This is the holographic image when recording

diffuse wavefronts. The intensity of this light over the intensity of the light illuminating the holographic material is known as Diffraction Efficiency, η, of the hologram. Normally, light reflected from the interfaces are first subtracted, to obtain a more accurate value of the real diffraction efficiency.

The importance of producing a hologram with a reasonable diffraction efficiency is obvious, whether the application is simply the viewing of a three-dimensional scene, holographic interferometry, or data storage; efficient use of the illuminating light allows for smaller and more economical systems.

The equations describing the diffraction efficiency of various hologram (grating) types are divided into two groups, those for plane holograms and those for volume holograms. This is because the description of the diffraction process for two cases is fundamentally different.

2.5.1. Thin Holograms:

For a thin amplitude grating hologram diffraction efficiency is given as [49]

$$\eta = \frac{0.188\alpha^2 M^2(\nu)}{K} \qquad (2.21)$$

where K is the beam ratio, $M(\nu)$ is the modulation transfer function of recording material at average spatial frequency ν, and α is slope of the amplitude transmittance-log exposure curve of recording material.

For a thin, lossless phase grating $|T_a(x)|=1$, the complex amplitude transmittance is

19

$$T_a = \sum_{n=-\infty}^{\infty} i^n J_n(\phi_v) e^{in\Phi} \qquad (2.22)$$

where J_n is the Bessel function of the first kind of order n. When a thin phase grating is illuminated, the light is diffracted into several orders. The diffracted amplitude in the nth order is proportional to the value of the Bessel function $J_n(\phi_v)$. Since only the first order is of interest in holography, the amplitude of the light diffracted into order 1 is proportional to $J_1(\phi_v)$ which has a maximum value of 0.58. Thus the maximum diffraction efficiency for a thin phase hologram is $(0.58)^2 =33.9\%$. This value is about five times higher than the diffraction efficiency obtainable for a thin amplitude grating, which makes the production of phase holograms desirable and attractive.

2.5.2. Thick Holograms:

The thick or volume hologram represents a very important hologram type since it is here where, at least theoretically, the maximum diffraction efficiency can be obtained. A special theory, known as coupled-wave theory has been developed by Kogelnik [51].

For pure phase holograms $n_0 = n + n_1 cos\left(\dfrac{2\pi x}{\Lambda}\right)$ and for pure amplitude holograms $\alpha_0 = \alpha + \alpha_1 cos\left(\dfrac{2\pi x}{\Lambda}\right)$, where Λ is the period of the grating, and α and n are the average values of the refractive index and the absorption constant, respectively. Therefore for thick phase transmission holograms, providing that the Bragg condition is satisfied is expressed by [51]

$$\eta_{tp} = sin^2\left(\frac{\pi n_1 d}{\lambda cos\theta_0}\right) \qquad (2.23)$$

where d is the thickness of the recording layer, λ the wavelength of the light, and θ_0 half angle between the recording reference and object beams.

When the Bragg condition is satisfied the diffraction efficiency for a pure phase reflection hologram is expressed by

$$\eta_{rp} = tanh^2\left(\frac{\pi n_1 d}{\lambda cos\theta_0}\right) \tag{2.24}$$

As a summary, the highest possible diffraction efficiencies obtainable for gratings are shown in Table 2.1.

Table 2.1. Theoretical maximum diffraction efficiencies for a grating hologram.

Hologram Type	Thin Transmission		Thick Transmission		Thick Reflection	
Modulation	Amplitude	Phase	Amplitude	Phase	Amplitude	Phase
Efficiency	6.25%	33.9%	3.7%	100%	7.2%	100%

CHAPTER III

HOLOGRAPHIC INTERFEROMETRY

Holographic interferometry is essentially a technique for the study of small displacements on the scale of wavelength of light. A wave recorded in a hologram is effectively stored for future reconstruction and use. Holographic interferometry is concerned with the formation and interpretation of fringe patterns which appear when a wave, generated at some earlier time and stored in a hologram, is later reconstructed and caused to interfere with a comparison wave [50]. It is the storage or time delay aspect which gives the holographic method a unique advantage over conventional interferometry. It permits diffusely reflecting or scattering surfaces which are subjected to stress to be interferometrically compared with their normal state.

Fringes characteristic of small displacements of a subject have relatively low spatial frequencies. Since interferometry is primarily concerned with such displacements, the term fringes refers to these low frequency patterns. Real-time, double-exposure, time-average, are descriptive labels attached to variants of this interferometric method.

3.1 Real-time Holographic Interferometry

In this technique, the hologram is replaced, after processing, in exactly the same position in which it was recorded [48]. When it is illuminated with the original reference beam, the virtual image coincides with the object. If, however, the shape of the object changes very slightly, two sets of light waves reach the observer, one being the reconstructed wave (corresponding to the object before the change) and the other the directly transmitted wave from the object in its present state. The two wave amplitudes will add at the points where the difference in optical path is zero or a whole number of wavelengths, and cancel at some other points in between. As a result, an observer viewing the reconstructed image sees it covered with a pattern of interference fringes, which is contour map of the change in shape of the object. These changes can be observed in real time.

Precise repositioning of the hologram after processing is necessary to avoid the introduction of spurious fringes. In addition, with photographic emulsions, it is necessary to take precautions to avoid local deformations of the emulsion due to non uniform drying. These problems can be avoided by exposing and processing the photographic plate in situ in a liquid gate. An alternative which completely eliminates the need for wet processing is to use thermoplastic recording.

3.2 Double-Exposure Holographic Interferometry

In double-exposure holographic interferometry, interference takes place between the wavefronts recorded by two holograms of the object recorded on the same photographic plate [48]. Typically, the first exposure is made with the object in its initial, unstressed condition, and the second is made with stress applied to the object. When the processed hologram is

illuminated with the original reference beam, it reconstructs two images, one corresponding to the object in its unstressed state, and other corresponding to the stressed object. The resultant interference pattern reveals the changes in shape of the object between the two exposures.

In this case, the intensity at the photographic plate during the first exposure is

$$I_1(x, y) = |r(x, y) + o(x, y)|^2 \qquad (3.1)$$

and that during the second exposure is

$$I_2(x, y) = |r(x, y) + o'(x, y)|^2 \qquad (3.2)$$

The amplitude transmittance of the resulting hologram is, therefore

$$t(x, y) = t_0 + \beta T(I_1 + I_2) \qquad (3.3)$$

When the hologram is illuminated once again with the same reference wave, the transmitted amplitude in the hologram plane is

$$u(x, y) = r(x, y)t(x, y) \qquad (3.4)$$

The only two terms of interest in the expansion Eq.(3.4) are those corresponding to the two superimposed primary images. The complex amplitude due to these is

$$u_3(x, y) = \beta T r^2 |o(x, y)| \{exp[-i\phi(x, y)] + exp[-i\phi'(x, y)]\} \qquad (3.5)$$

so that the resultant intensity is

$$I_3(x, y) \propto |o(x, y)|^2 \{1 + cos[\Delta\phi(x, y)]\} \qquad (3.6)$$

where $\Delta\phi(x, y) = \phi(x, y) - \phi'(x, y)$ is the phase difference between the wavefronts, which gives rise to the fringes seen by the observer. In this case the hologram is a permanent record of the change in shape of the object. For a diffusely reflecting object $\Delta\phi$ is given as shown in Figure 3.1 by the relation

$$\Delta\phi = (\bar{k}_2 - \bar{k}_1) \cdot \bar{L} \qquad (3.7)$$

where $\bar{k}_1$ and $\bar{k}_2$ are the propagation vectors of incident and scattered light with magnitude $|\bar{k}_1| = |\bar{k}_2| = k_0 = 2\pi / \lambda$ and taken along the directions of illumination and observation respectively.

For transparent objects, the relationship between the displacements of interference fringes and refractive index is simplest when the object is homogenous along the line of observation, i.e., the refractive index depends only on the co-ordinates x and y and does not depend on z (two dimensional distribution). Then

$$\Delta\phi(x, y) = \frac{2\pi t}{\lambda}[n(x, y) - n_0] \qquad (3.8)$$

where $t = Z_2 - Z_1$ is the thickness of the layer being studied.
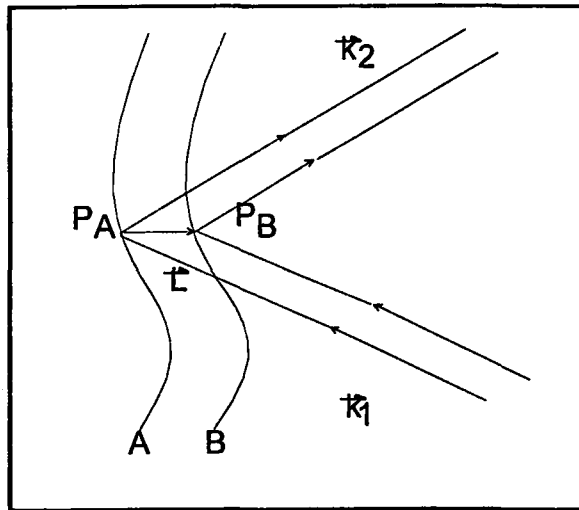
Figure 3.1. Calculation of phase difference in the interference pattern.

Double-exposure holographic interferometry is much easier than real-time holographic interferometry, because the two interfering waves are always reconstructed in exact register. Distortions of the emulsion affect both images equally, and no special care need to be taken in illuminating the hologram when viewing the image. In addition, since the two diffracted wavefronts are similarly polarised and have almost the same amplitude, the fringes have very good visibility.

However, double-exposure holographic interferometry also has certain limitations. The first is that where the object has not moved between exposures, the reconstructed waves, both of which have experienced the same phase shift, add to give a bright image of the object. This makes it difficult to observe small displacements. A dark field, which gives much higher sensitivity, can be obtained by holographic subtraction. For this the phase of the reference beam is shifted by π between the two exposures. Another limitation is that information on intermediate states of the object is lost.

3.3 Difference Holography

In holography, it is impossible to compare two objects to measure differences in their deformations or shapes. To determine, for example, the difference in deformation of two objects due to the same load, each displacement field has to be separately calculated, and only then can numerical results can be compared. As a consequence of high sensitivity of holographic interferometry, large displacements can not be measured because of unresolvable interference patterns. Difference holographic interferometry (DHI) overcomes the difficulties described above, producing a comparing technique for measurement of displacement fields and shapes of different objects with complicated surfaces. It works without needing to consider different microstructures of object surfaces.

Let us produce two coherent wavefields with a phase difference of given spatial distribution in a proper way. They will be referred to as master wavefronts. Using master wavefronts for illumination, a double exposure interferogram of the object to be investigated has to be recorded. Between the two new object wavefronts scattered by the object and caused by its displacement there exists a phase difference with characteristic spatial distribution. At the reconstruction of the double exposure interferogram, the wavefronts representing the phase differenced overlap and their sum or /and difference can be displayed. Difference interference pattern can be observed if the phase differences are of opposite sign.

Master wavefronts with arbitrary phase difference, reflecting reference or master displacement, can be produced and stored, recording a double exposure interferogram of a master object. Wavefronts illuminating the object to be compared can be produced by wavefront reversal, reconstructing the master interferogram by conjugate reference beam(s)

used during the recording process. The techniques of DHI have been reviewed in ref. [52].

The flow chart of single reference beam technique is shown in Figure 3.2. The symbols U_{M1} and U_{M2} denote the complex amplitudes of the conjugated master wavefronts which can be generated by reconstruction of the master hologram H by the reversed reference beam. The two wavefields illuminate the test object simultaneously in its initial and final states as discussed above. The complex amplitudes of the test object beams at the (new) plate H' are denoted U_1 and U_2.

The test holograms are recorded on the plate H by the reference beam r. The irradiance of the reconstructed images of the test object during reconstruction can be obtained as
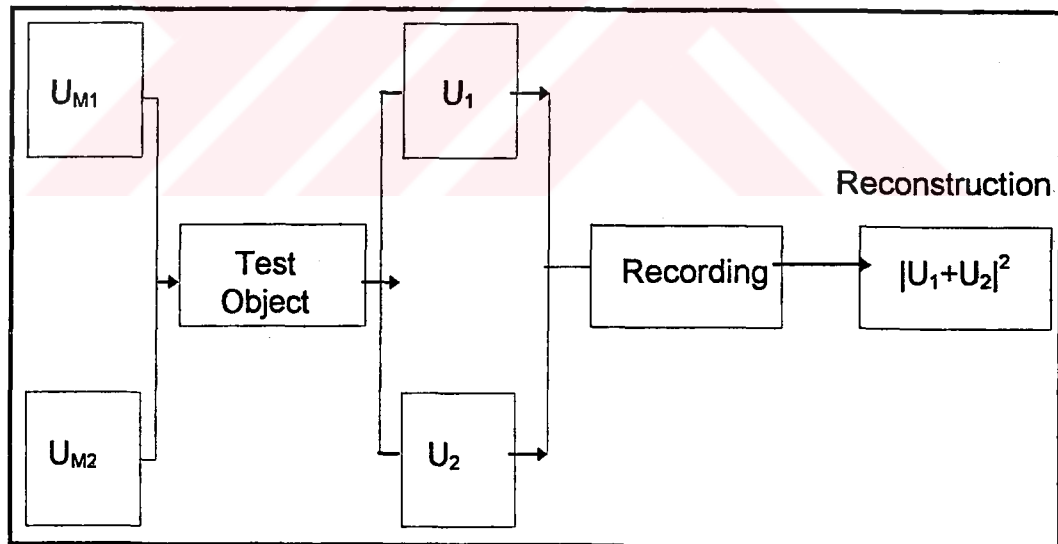
Figure 3.2. The flow chart of the single reference beam technique.

$$I = \left(\bar{U}_1 + \bar{U}_2\right)^2 \qquad (3.9)$$

The complex amplitude U_1 and U_2 of light arriving at the plate H' in the two exposures may be expressed as

$$U_1 = U_0 \exp\left(i\phi_0\right) + U_0 \exp\left[i\left(\phi_0 + \Delta\phi\right)\right] \qquad (3.10)$$

and

$$U_2 = U_0 \exp\left[i\left(\phi_0 + \Delta\phi'\right)\right] + U_0 \exp\left[i\left(\phi_0 + \Delta\phi + \Delta\phi'\right)\right] \qquad (3.11)$$

Eqs. (3.10) and (3.11) refer to the initial and final states of the test object, respectively. The first terms on the right of both equations correspond to the illumination by the real image of the unloaded master object while the second terms correspond to that of the loaded master. The symbols $\Delta\phi$ and $\Delta\phi'$ are functions of the spatial co-ordinates at the plate. Substituting Eq. (3.10) and (3.11) into Eq. (3.9) we get after rearranging the terms:

$$I = U_0^2\left[4 + 4\cos\Delta\phi + 4\cos\Delta\phi' + 2\cos\left(\Delta\phi + \Delta\phi'\right) + 2\cos\left(\Delta\phi - \Delta\phi'\right)\right] \qquad (3.12)$$

The modulation of the irradiance is determined by the 2nd - 5th terms. The second term describes the interference pattern related to the master object deformation, the third one that of the test object deformations. The sum and difference of the two interference patterns are equally present (4th and 5th terms).

The interference pattern described by the expression Eq.(3.12) can easily be interpreted only when the phase differences $\Delta\phi$ and $\Delta\phi'$ are sufficiently large to produce interference fringe systems of high spatial frequency (not observable). Then, only the difference interference fringes

are visible. The high frequency master and test interference patterns and their sum, lead to a decrease in the visibility of the difference interference pattern. The visibility can be improved by optical or digital filtering.

A simple interpretation of formation of difference interference pattern can be given as follows [53-54]; Let the well-known expression in holographic interferometry

$$\Delta\varphi = \left(\vec{k}_2 - \vec{k}_1\right).\vec{L} \tag{3.13}$$

belong to the master object displacement field, where $\vec{k}_1$ and $\vec{k}_2$ are illumination and observation vectors, respectively, having magnitude $2\pi/\lambda$. $\vec{L}$ is the displacement vector at the object surface point considered. The phase difference $\Delta\varphi$ was previously referred to as that between master wavefronts.

Now the master object is taken away from the arrangement used for recording the master holograms. In an such arrangement a new double exposure interferogram can be recorded, while illumination beams are produced by wavefront reversal and the photosensitive plate is placed along the direction of the beam illuminating the master object during the recording of master holograms.

The structure of interference pattern recorded in such a way can be interpreted by analysis of Figure 3.3, where A' and B' are the initial and final positions of an object to be compared. PA' and PB' are positions of an object surface point before and after loading; $-\vec{k}_2$ and $-\vec{k}_1$ are illumination and observation vectors, respectively; and $\vec{L}'$ is the displacement vector.

30
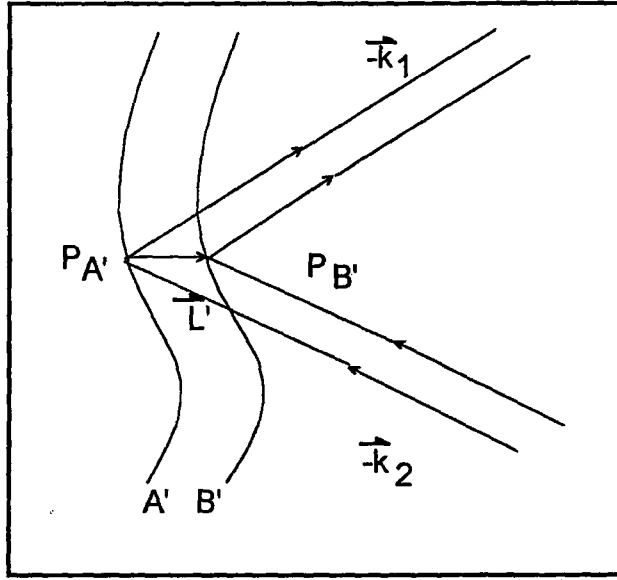
Figure 3.3. Formation of difference interference pattern.

Using master wavefronts for illumination in original sequence, the phase difference $\Delta\varphi_-$, corresponding to the difference of $\Delta\varphi$ belonging to the master object (see Eq. 3.13), and

$$\Delta\varphi' = \left[\left(-\vec{k}_1\right) - \left(-\vec{k}_2\right)\right].\vec{L}' \tag{3.14}$$

determining the displacement field of the object under investigation at a given geometry, will directly show the difference of displacements $\vec{L}$ and $\vec{L}'$. It can be expressed using Eq.(3.13) and Eq.(3.14) in a form

$$\Delta\varphi_- = \Delta\varphi' - \Delta\varphi = \left(\vec{k}_2 - \vec{k}_1\right)\left(\vec{L}' - \vec{L}\right) \tag{3.15}$$

Using illuminating master wavefronts in reversed sequence, the sum of displacements $\vec{L}$ and $\vec{L}'$ can be measured. It is reflected by the following expression

$$\Delta\varphi_+ = \Delta\varphi' + \Delta\varphi = \left(\vec{k}_2 - \vec{k}_1\right)\left(\vec{L}' + \vec{L}\right) \tag{3.16}$$

31

CHAPTER IV

OPTICAL SYSTEMS AND LIGHT SOURCES

Making a hologram involves recording a two-beam interference pattern. The principal factors which must be taken into account in a practical set-up to obtain a good result are discussed in this chapter.

4.1. Vibration Isolation

Any change in the phase difference between the two beams during the exposure will result in a movement of fringes and reduced modulation in the hologram [48]. Most commonly, to avoid mechanical disturbances, all the optical components as well as the object and recording medium are mounted on a stable surface. Acceptable results can be obtained with a concrete slab resting on a inflated scooter inner tubes, but most laboratories now use a rigid optical table supported by a pneumatic suspension system, so that it has a low natural frequency of vibration (~1Hz). Air currents, acoustic waves and temperature changes also cause major problems. Their effects are usually minimised by enclosing the working area.

Residual disturbances can be eliminated almost completely by a feedback system in which any motion of interference fringes in the hologram plane is picked up by a photodetector. Variations in its output are amplified

and applied to a piezoelectric element which controls the position of a mirror in the reference beam path to restore the path difference between the two beams to its original value.

4.2. Fringe Visibility

To produce a hologram that reconstructs a bright image, the interference pattern formed at the recording medium by the object and reference waves should have as high a contrast as possible. This is because the amplitude of the diffracted wave increases with the modulation depth of the interference pattern recorded.

The contrast of the interference pattern at any point in the hologram plane is measured by the fringe visibility which is given by the relation

$$V = \frac{I_{max} - I_{min}}{I_{max} + I_{min}} \tag{4.1}$$

where I_{max} and I_{min} are the local maximum and minimum values of the intensity.

4.3. Beam Polarisation

Most gas lasers used for holography have Brewster angle windows on the plasma tubes so that output beam is linearly polarised. Maximum visibility of the fringes will then be obtained if the angle ψ between the electric vectors in the two interfering beams is zero. This condition is automatically satisfied, irrespective of the angle between the two beams, if

they are both polarised with electric vector normal to the plane of the optical table. On the other hand, if they are polarised with the electric vector parallel to the surface of the table, the angle ψ between the electric vectors is equal to the angle θ between the two beams, and, in the extreme case where the two beams intersect at right angles, the visibility of fringes drops to zero.

With a diffusely reflecting or metallic object it is also necessary to take into account the polarisation changes in the light scattered by it which can result in a significant decrease in the visibility of fringes. This can be minimised either by rotating the polarisation of the reference beam so that the cross-polarised light can also interfere with it, or by using a sheet polariser in front of the hologram plate to eliminate the cross-polarised component. Another alternative is to use a circularly polarised reference beam.

4.4 Beam Splitters

If we assume that the interfering beams are polarised with the electric vector perpendicular to the plane of incidence, the fringe visibility is given by the relation

$$\Gamma = 2\left|\gamma_{12}(\tau)\right| \text{or} / \left(o^2 + r^2\right) \tag{4.2}$$

where r and o are the amplitudes of the reference and object beams, and $\gamma_{12}(\tau)$ is the degree of coherence between them. If the beam ratio, $R = (r/o)^2$, is defined as the ratio of irradiances of the reference and object beams, Eq.(4.2) can be written as

$$\Gamma = 2\left|\gamma_{12}(\tau)\right| R^{1/2} / (1 + R) \tag{4.3}$$

The fringe visibility is obviously a maximum when R=1. However, the wave scattered by a diffusely reflecting object exhibits quite strong variations in amplitude. Hence, in hologram recording it is usually necessary to work with a value of R>>1 to avoid non-linear effects.

To optimise the visibility of the fringes at the hologram plane it should be possible to vary the ratio of the power in the beam illuminating the object to that in the reference beam. A convenient way to do this is to use a beam splitter consisting of a disc coated with a thin aluminium film whose reflectivity is a linear function of the azimuth.

4.5. Beam Expansion

The laser beam has to be expanded to illuminate the object and the plate on which the hologram is recorded. Usually this is done with microscope objectives.

If the laser is oscillating in the TEM_{00} mode, the beam has a Gaussian profile so that the amplitude at a point at a radial distance r from the centre of the beam is

$$a(r) = a(0)\,exp\left(-r^2 / w^2\right) \tag{4.4}$$

where a(0) is the amplitude at the centre of the beam and w is the beam radius (the radius at which the amplitude drops to 1/e of its maximum value).

Accordingly, P(r) the laser power within a circle of radius r is given by the relation

$$P(r) = \int_0^r I(r)2\pi r dr \tag{4.5}$$

where $I(r)=|a(r)|^2$ is the intensity at a radial distance r from the centre of the beam; this can be written as

$$P(r) = P_{tot}\left[1 - exp\left(-2r^2 \, / \, w^2\right)\right] \qquad (4.6)$$

where P_{tot} is the total power in the beam. From Eq. (4.4) and Eq. (4.6) it follows that

$$\frac{P(r)}{P_{tot}} = 1 - \left[\frac{I(r)}{I(0)}\right] \qquad (4.7)$$

This is a useful relation giving the loss in power that must be tolerated for a given degree of uniformity of illumination.

Due to the high coherence of laser light, the expanded beam invariably exhibits diffraction patterns (spatial noise) due to scattering from dust particles on the optical surfaces in the beam path. To eliminate these, a pinhole is placed at the focus of the microscope objective. If this pinhole has a radius ρ, spatial frequencies higher than $\xi=\rho/\lambda f$, where λ is the wavelength of the light and f is the focal length of the microscope objective, are blocked. These higher spatial frequencies mainly represent noise, so that the transmitted beam has a smooth Gaussian profile.

A proper choice of the size of the pinhole can ensure that the power loss is minimal. Thus, it follows that the amplitude in the focal plane of the microscope objective, obtained from the two-dimensional Fourier transform of Eq.(4.4) is

$$A(\rho) = A(0) \, exp\left(-\pi^2 w^2 \rho^2 \, / \, \lambda^2 f^2\right) \qquad (4.8)$$

36

where ρ is the radial distance from the centre of the beam. A schematic diagram of spatial filter and collimator system is shown in Figure 4.1.
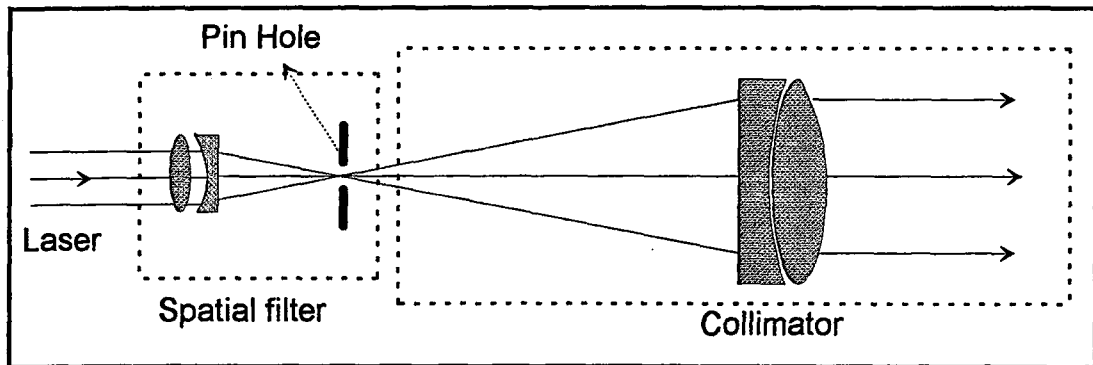
Figure 4.1. Schematic diagram of spatial filter and collimator system.

Typically, with an argon-ion (Ar^+) laser, λ=514 nm and w=0.8 mm, and with a 16 mm microscope objective and a 10μm diameter pinhole, the amplitude at the edge of the pinhole is only 0.08 of that of at the centre. Hence, from Eq.(4.8), more than 99 percent of the total power in the beam is transmitted through the pinhole.

4.6. Exposure Control

An accurate spot photometer is required to measure the irradiances due to the object and reference beams in the hologram plane, so as to set the beam ratio R at a suitable value. Because of the limited dynamic range of photographic materials used for holography, the object illumination should be adjusted so that the irradiance in the hologram plane due to it is reasonably uniform. In addition, precise control of the exposure is required to ensure good diffraction efficiency and avoid non-linear effects. To overcome this problem it is convenient to use an electronic exposure-

control unit which integrates the irradiance in the hologram recording plane and closes the shutter at a pre-set value of radiant exposure.

4.7. Coherence Requirements

In order to obtain maximum fringe visibility, it is also essential to use a coherent light source. Gas lasers provide an intense source of highly coherent light and therefore used almost universally in optical holography.

Spatial coherence is automatically ensured if the laser oscillates in a single transverse, preferably the lowest order or TEM_{00} mode, since this is inherently the most stable and gives most uniform illumination over the field. Normally, this is no problem since most gas lasers are designed to operate in this mode. However, they are not usually designed for single-frequency operation, which would imply that they should also oscillate in only one longitudinal mode. The temporal coherence of most lasers is therefore limited by their longitudinal mode structure.

To obtain a satisfactory hologram, the maximum optical path difference between the object and reference beams in the recording set-up must be less than the coherence length of the light from the laser.

4.8. Temporal Coherence of Laser

The simplest form of resonant cavity for a laser is made up of a pair of mirrors separated by a distance L, through in some cases, where operation on more than one line is possible, a wavelength selector prism may also be necessary as shown in Figure 4.2. The resonant frequencies of such a cavity are given by the expression

$$\nu_n = n(c/2L) \qquad (4.9)$$

where n is an integer and c is the speed of light. However, as shown in Figure 4.3, the laser can oscillate only at those frequencies within the gain curve of the active medium at which the gain is adequate to overcome the cavity losses.
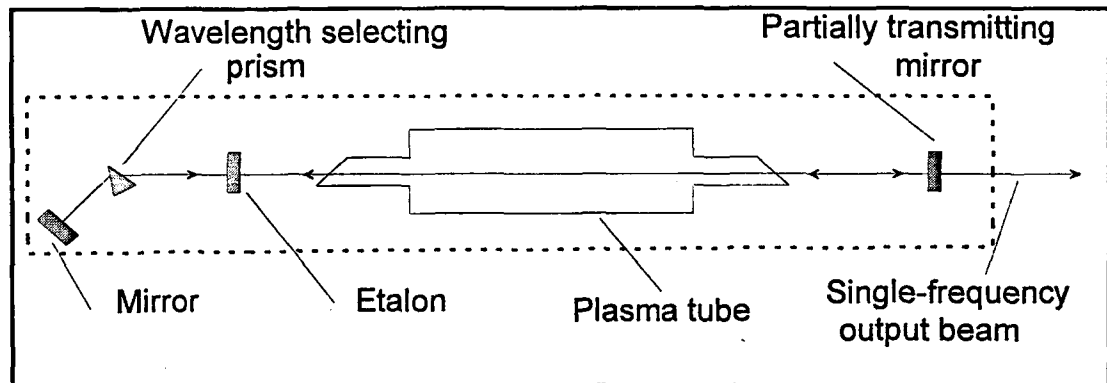
Figure 4.2. Optical system of a typical Ar^+ Laser.

The width of the individual modes depends on the losses as well as the mechanical stability of the cavity structure and is typically about 3 MHz. Accordingly, if a laser is made to oscillate in a single longitudinal mode, the coherence length would be of the order of 100 meters.

Since, in frequency space, the width of the individual modes is less than their separation (which may range from 600 MHz for a 25 cm cavity down to 75 MHz for a 2m cavity), the power spectrum of a laser oscillating in N longitudinal modes can be represented by N equally spaced delta functions. If we assume that the total power is divided between the N modes, the power spectrum can be written as

$$S(v) = \sum_{n}^{n+N-1} \delta(v - v_n)$$ (4.10)

The degree of temporal coherence of such a source for a path difference **p** can be written as [48]

$$\gamma_{12}(p) = \left| \frac{sin(N\pi p / 2L)}{N sin(\pi p / 2L)} \right|$$ (4.11)
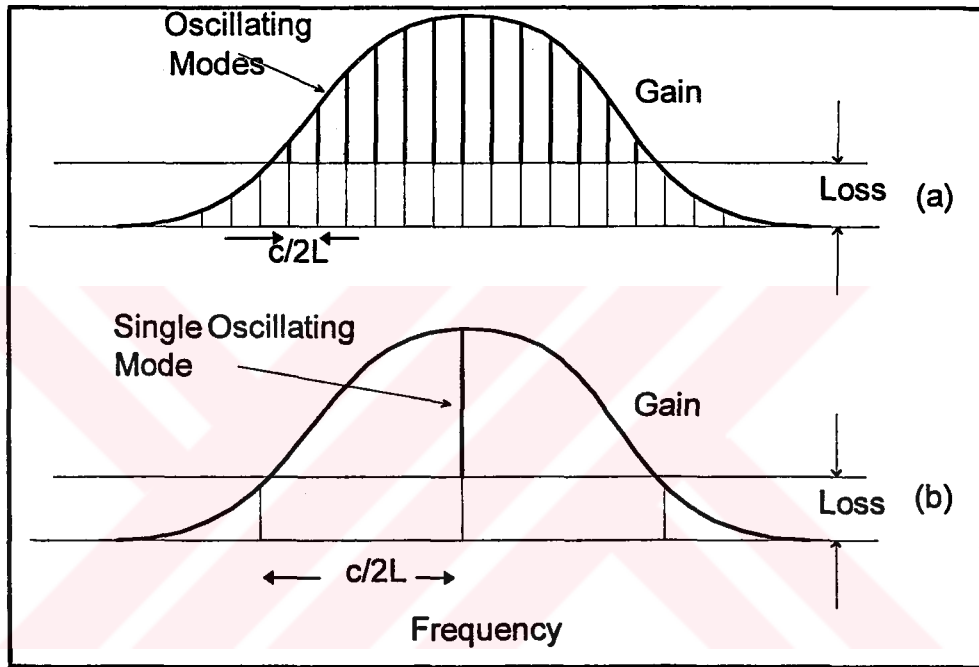
Figure 4.3. Oscillation frequencies of laser with (a) a long resonant cavity and (b) a short resonant cavity.

This is a periodic function whose first zero occurs when

$$p = 2L/N$$ (4.12)

corresponding to the effective coherence length. Fringes with acceptable visibility can usually be obtained for path differences that are less than half the coherence length.

It is apparent from Eq.(4.12) that the existence of more than one longitudinal mode reduces the coherence length of a laser severely. A short coherence length is troublesome, since it makes it essential to equalise the mean optical paths of the object and reference beams and restricts the maximum depth of the object field that can be recorded.

The simplest way to force a laser to operate in a single longitudinal mode is to use a very short cavity so that the spacing of the longitudinal modes is greater than the width of the gain profile over which oscillation is possible. This occurs when

$$c/2L \geq \Delta v \tag{4.13}$$

where Δv is the width of the gain profile (typically 1.7 GHz for He-Ne laser, 3.5 GHz for an Ar^+ laser). However, the power available from such a short cavity is extremely limited.

The most common method of ensuring single frequency operation is to use a intercavity etalon as shown in Figure 4.2. In effect the laser is now made up of two resonant cavities, and only those modes which are common to both cavities, as shown in Figure 4.4, have low enough losses for oscillation to be possible. If the length of the etalon is made short enough that it satisfies Eq. (4.13), it can support only one mode, and single-frequency operation is obtained.

If the etalon is to act as a simple transmission filter, it must be tilted to decouple it from the laser cavity. It can be tuned to maximise the

41

output power by tilting it further so that its resonant frequency corresponds to the peak of the gain curve.
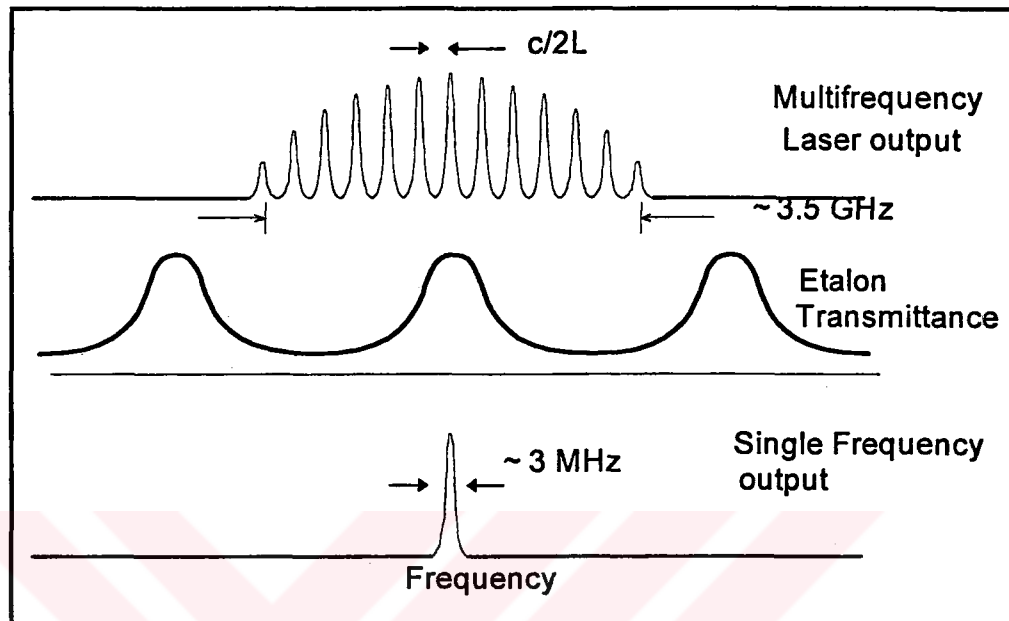
Figure 4.4. Normal multifrequency output, etalon transmittance and single frequency output with an intercavity etalon for a typical Ar^+ laser.

4.9. Gas Lasers

The light source most commonly used in holography is a gas laser. Gas lasers, in general, are cheaper, easier to operate and have better coherence characteristics than other types of lasers. The range of useful wavelengths and typical output powers available at these wavelengths with the most commonly used gas lasers are summarised in Table 4.1.

When working with any laser, adequate safety measures must be taken to avoid eye damage. Even with relatively low power gas lasers

($\approx$1mW) the beam should not enter the eye directly. This is because the beam is focused into very small spot on the retina resulting in a power density about 10^5 times that at the cornea.

Table 4.1. Output wavelength and output power of typical gas lasers

Wavelength, nm	Laser	Typical Power, mW	Colour
442	He-Cd	25	Violet
458	Ar+	200	Blue-violet
476	Kr+	50	Blue
477	Ar+	400	Blue
488	Ar+	1000	Green-Blue
514	Ar+	1400	Green
521	Kr+	70	Green
633	He-Ne	2-50	Red
647	Kr+	500	Red

For simple holographic set up, the He-Ne laser is far the most economical choice. It operates on a single line at 633 nm, does not require water cooling and has a long life. However, depending on their power, commercial He-Ne lasers oscillate in three to five longitudinal modes, and the coherence length is limited.

In contrast to the He-Ne laser, the Ar^+ laser essentially has a multiline output but can be made to operate on a single line by replacing the reflecting end mirror by a prism and mirror assembly. It is also relatively easy to obtain singe-frequency operation with an etalon. Argon-ion lasers can give high power output and an extended coherence length in the blue or green regions of the spectrum, the two strongest lines being at 488 nm and 514 nm.

4.10 Scanning Interferometer

Figure 4.5. shows a typical scanning confocal interferometer. It consist of two spherical mirrors, separated by a distance equal to their radius of curvature. The back surfaces of the mirrors are made such that the mirrors are self-collimating, i.e., a plane wavefront incident on the interferometer will be transformed into a spherical wavefront whose radius of curvature matches that of transverse modes of the interferometer. The interior concave surfaces of the mirrors are coated with high reflectance multilayer films, and the external convex surfaces are coated with anti-reflection films to eliminate spurious interferometer resonances involving the back surfaces of the mirrors.

The mirrors are mounted in cells which are separated by a piezoelectric spacer. By applying a potential difference of a few hundred volts to the piezoelectric spacer, the separation of the mirrors can be varied by a few wavelengths of light. In practice, sawtooth waveform is usually applied to the piezoelectric spacer to vary the separation of the interferometer mirrors linearly as a function of time. For a confocal interferometer, a change in separation of the mirrors of one-fourth wavelength scans the interferometer through one free spectral range.
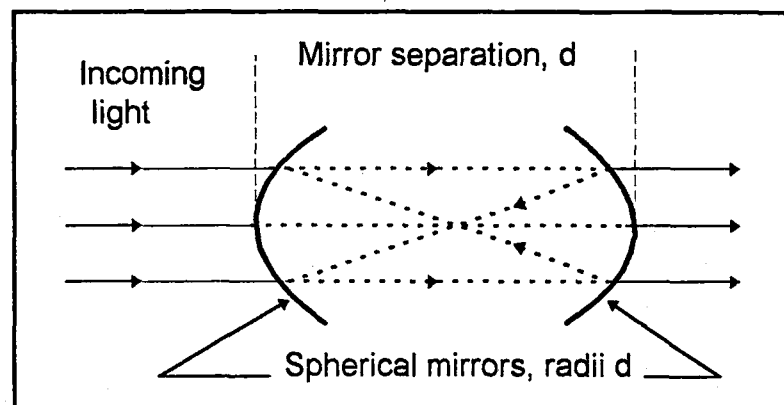
Figure 4.5 Spherical mirror Fabry-Perot interferometer.

44

The light transmitted by the interferometer is detected by a photocell, and output signal is recorded on an oscilloscope as a function of the voltage applied to the piezoelectric spacer. The oscilloscope thus displays a signal which is roughly equivalent to the laser mode intensity vs. optical frequency. A number of characteristics of a spherical mirror Fabry-Perot interferometer are illustrated by the transmission vs. frequency curve, Figure 4.6.

The Free Spectral Range (FSR) of an interferometer is the separation between corresponding transmission maxima of adjacent orders, hence the maximum spectral bandwidth of incoming light which can be observed without overlapping orders (optical frequencies other than those which fall within one free spectral range of interferometer). Expressions for the free spectral range of a confocal spherical mirror interferometer of spacing d is given by
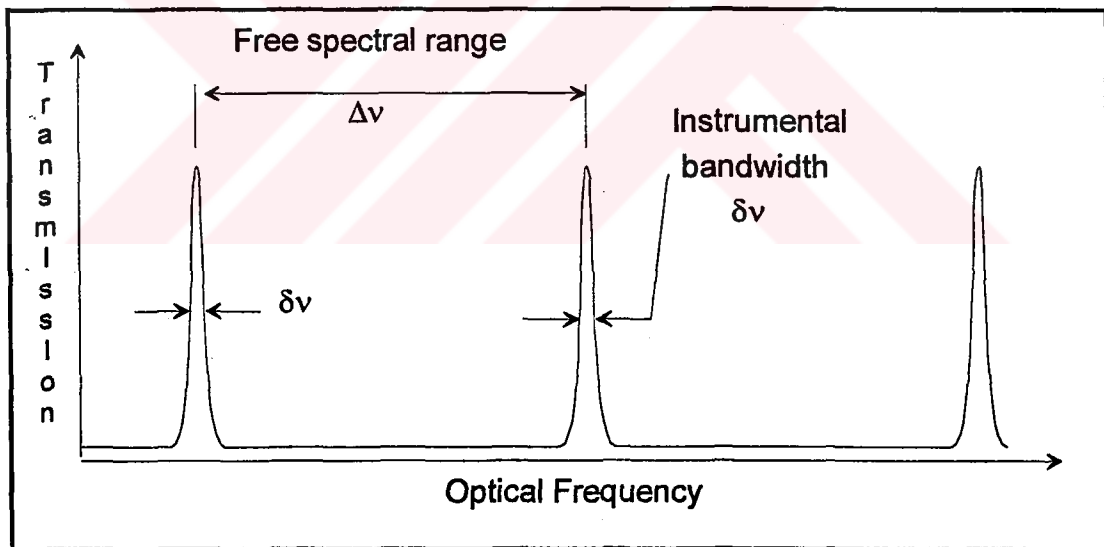
Figure 4.6 Transmission vs. frequency of a Fabry-Parot interferometer.

$$\Delta v = \frac{c}{4d}$$

The apparent or observed spectral width of a true monochromatic spectral line is shown in Figure 4.6 identified as δv, instrumental bandwidth.

The finesse of a multiple-beam interferometer may be defined as the ratio of the free spectral range to the instrumental bandwidth. It is a fundamental measure of the spectral resolving capability of the instrument. The finesse may be interpreted as the effective number of beams contributing to the multiple beam interference, and is analogous to the number of grooves on a diffraction grating.

$$F = \frac{\Delta v}{\delta v}$$

The finesse of an instrument is determined by a number of factors, among which are the reflectivity (R) of the mirrors and the surface figure of mirrors and given as, for a confocal geometry,

$$F \approx \frac{\pi}{2(1-R)}$$

4.11 Scanning Probe Microscope (SPM)

Several techniques are available for magnifying the detailed features of a surface. Methods for magnifying surface features originated with magnifying lenses and optical microscopy in the late 18th century. During the 20th century, the methods for magnification based on electron and ion beams were developed. Table 4.2 compares magnification, operating environment, type of image and damage to sample [55-56]. The

first four techniques listed in the table rely on focusing particles such as photons, electrons, and ions to resolve an image. Optical instruments are limited by the wavelength of the visible light and resolve down to approximately 0.5 microns. The scanning electron microscope (SEM), which operates only in vacuum, can resolve nanometer features if there is high atomic number contrast, but with possible destructive effects on the surface. Depth information is not readily obtained by SEM.

The scanning probe microscope is a recent innovation that relies on a mechanical probe for generation of magnified images. A SPM is operable in ambient air, liquid or vacuum to resolve features in three dimensions down to a fraction of an angstrom. A SPM is comprised of a sensing probe, piezoelectric ceramics, a feedback electronic circuit, and a computer for generating and presenting images.

Table 4.2. Magnification techniques

System	Mag. Factor	Medium	Image	Damage
Optical	10^3	Air, Liquid	2-D	None
Laser Scan	10^4	Air	2-D	Minimal
Ion Beam	10^5	Vacuum	2-D	Severe
SEM	10^6	Vacuum	2-D	Some
SPM	10^9	Air, Liquid, Vacuum	3-D	Minimal to None

4.11.1 Force Sensor (AFM)

The force sensor, Figure 4.7, measures the deflection of a cantilever.
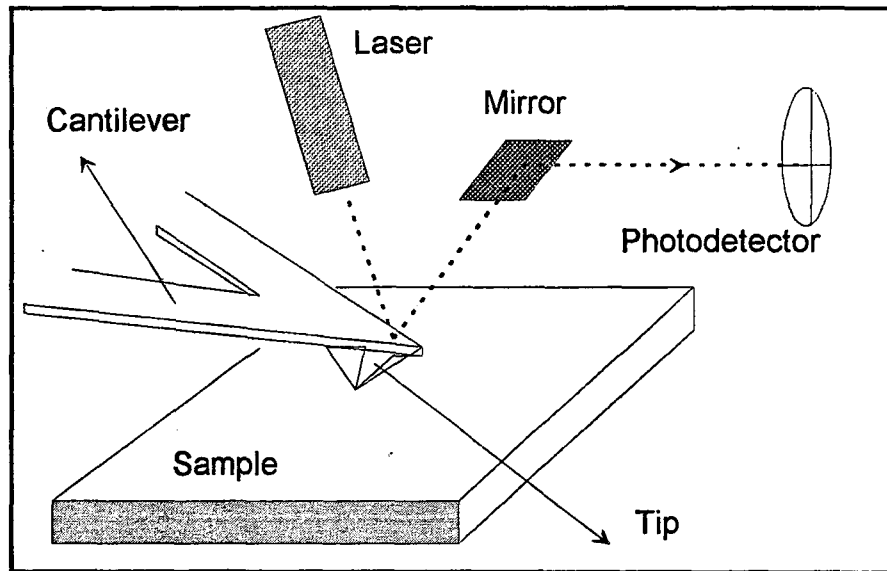
Figure 4.7. Schematic diagram of a force sensor.

A tip is mounted on the cantilever such that, when the cantilever moves, the light beam from a small laser moves across the face of a four section (quadrant) photo detector. The amount of motion of the cantilever can be calculated from the difference in light intensity on the sector. Hook's Law gives the relationship between the cantilever's motion, x, and the force required to generate the motion, F.

$$F=-kx$$

It is possible to fabricate a cantilever with a force constant, k, of 1 newton/meter. Since motion of less than 1 angstrom can be measured, forces less than 0.1 nanonewton are detectable.

4.11.2 Piezoelectric Ceramics

The control of the SPM sensor over extremely small distances is made possible by the use of piezoelectric ceramics. Ceramics are fabricated

into a variety of shapes and configurations. Each type of ceramic has a unique expansion coefficient that allows the calculation of physical distortion upon the application of a potential. The coefficients range from 1 angstrom/volt to 3000 angstrom/volt. As a result, these ceramics permit the accurate positioning of the probe tip.

4.11.3 SPM Instruments

A feedback electronic circuit is combined with a probe/sensor and piezoelectric ceramics to create the positioning mechanism. With this positioning mechanism the sensor can be maintained at a fixed distance from the surface. When the sensor moves toward the surface the output of the sensor electronics increases. The differential amplifier compares the increased value from the sensor electronics to the reference value (Vs) and outputs a correction voltage. The correction voltage excites the piezoelectric ceramic such that the sensor is pulled away from the surface. By adding two ceramics to scan the sensor in the X-Y plane and a computer to capture the error signal from the integrator to the positioning device the microscope, Figure 4.8, is created. An image of a surface is generated by rastering the sensor over the surface and storing the piezo driver signal on the computer.

A scanning probe microscope magnifies in three dimensions, the x, y, and z axes, and the maximum resolution in each of these axes is determined by different factors. Resolution in the z-axis in a scanning probe microscope is limited by the level of vibrations between the probe and surface. The maximum achievable resolution in the plane formed by the x and y axes is established by the geometry of the probe itself. When imaging extremely flat surfaces this is determined by the diameter of the atom (or atoms) at the probe's tip. Thus, the macroscopic probe tip structure is not

critical in atomic resolution imaging. When imaging large surface features, however, image quality is determined by probe geometry.
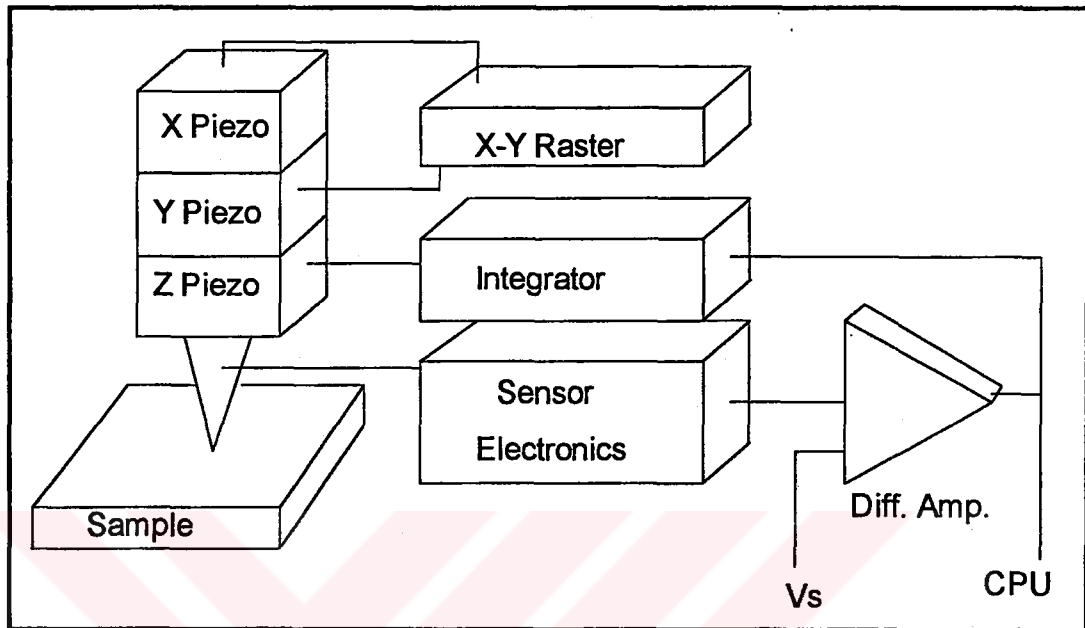
Figure 4.8 Scanning probe microscope system.

Imaging modes can be classified as "contact" or "non-contact" depending on the net forces between the probe and sample When the AFM is operating in the attractive region, it is called "non-contact". In this region, the AFM cantilever is curved toward the sample, since it is being pulled by attractive forces. Operation in the repulsive region is called "contact" imaging, and cantilever is curved away from the sample due to the repulsive forces. These imaging modes take place in different parts of the force/distance relationship, as shown in Figure 4.9.

The standard method of AFM imaging is the DC contact method. In this method force is repulsive and cantilever is soft. The displacement of probe is used by the feedback loop to adjust the z-piezoelectric ceramic so that the force between the probe and sample stays constant. The voltage
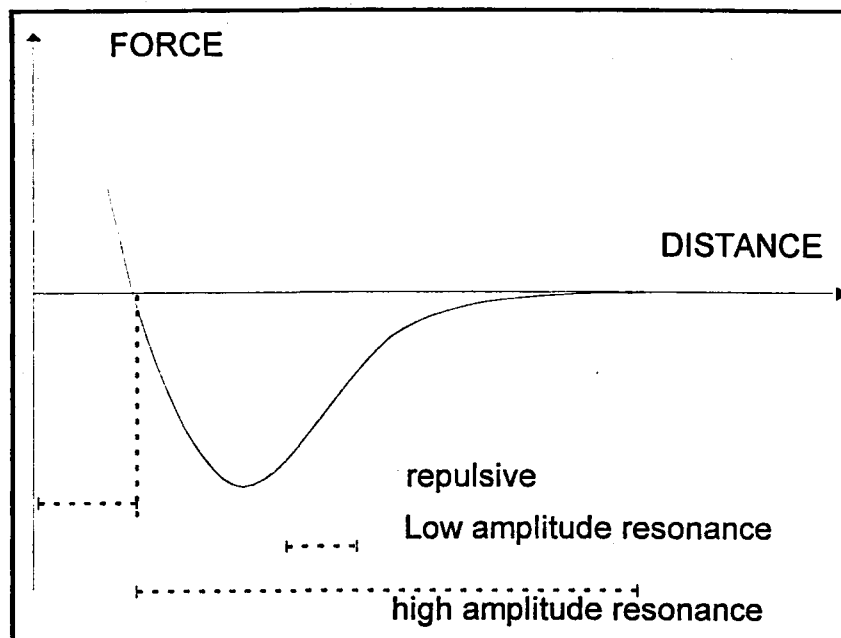
Figure 4.9. Operating regimes of different scan modes.

required to do this is used as the z data for imaging. This is called "constant force", or "slow scan" mode. If the scan is done very fast (or the feedback loop is slowed), the z-piezoelectric ceramic will not be able to keep up with features in the sample surface: in this case, the sensor output (from deflection of cantilever) is used as z-data. This mode is called "variable force", or "fast scan". Contact mode is useful for a wide range of applications. It can be used for both hard and soft samples, although soft samples require use of a weak cantilever and light sources, it is simple to operate.

CHAPTER V

RECORDING MATERIALS

The main branches of holography; interferometry, optical information processing, synthesis of optical elements impose a considerable number of serious requirements that hologram recording materials must meet. These requirements are often of a specific nature and relate only to a given specific application, being much smaller in importance for other applications.

The ideal recording material for holography should have a spectral sensitivity well matched to available laser wavelengths, a linear transfer characteristic, high resolution, low noise and high diffraction efficiency. In addition, it should either be indefinitely recyclable or relatively inexpensive[48].

5.1 Optical Changes in Photosensitive Materials

Exposure and (if necessary) development of a photosensitive material must alter the optical transmission properties of the material if it is to be useful for forming holograms[50]. Let us briefly consider a wave propagation in a homogeneous lossy medium. A plane wave, having propagated a distance d through a medium, emerges with a complex amplitude

$$U=U_0\exp(-\gamma d)$$
$$=U_0\exp(-i\beta d)\exp(-\alpha d) \tag{5.1}$$

where $\beta=2\pi n_0/\lambda_a$ is the propagation constant, α is the absorption constant, n_0 is the index of refraction, and $\alpha \ll \beta$. The exponential factors can thus be written

$$U/U_0=\exp(-\alpha d)\exp(-i(2\pi n_0 d/\lambda_a)) \tag{5.2}$$

If a material is to be considered for holographic recording, it must respond to exposure and development with a change in at least one of the parameters α, n_0, or d. It is the case that only one parameter changes significantly. We can therefore categorise most useful photosensitive materials as (a) amplitude modulating or absorption materials if α is exposure dependent and (b) phase modulating or phase materials if either n_0 or d is exposure dependent.

5.2 Absorption Materials

Holographic interference fringes are recorded in an absorption material as a spatial variation of its light absorption. Silver halide photographic emulsion and photochromic glasses and plastics are examples of this type of material. In the case of a homogeneous absorption material whose absorption constant is α and whose thickness in the direction of an incident plane wave is d, we can define the following quantities

Amplitude transmittance : $T=\exp(-\alpha d)$

Optical density : $D=\log(T^2)=2\alpha d\log_{10}(e)=0.869\alpha d$

To obtain maximum diffraction efficiency from a elementary plane transmission hologram with sinusoidal fringes, T should vary sinusoidally between 0 and 1. In practice this is difficult to achieve since corresponding range in optical density would be $\infty > D > 0$. A maximum density of D=2 yielding a transmittance T=0.1 is sufficient and easily achieved with photographic emulsion. The theoretical optimum average density of plane hologram should be D=0.6 [13].

5.3 Phase Materials

Holographic fringes are recorded in a phase material as a spatial modulation of either refractive index n or thickness d. Phase material is usually nearly transparent so that the absorption constant $\alpha \approx 0$. The difference in the phase of the light transmitted through a dielectric slab of thickness d and index n_0 compared to that transmitted through an equal thickness of air is given by as

$$\varphi = 2\pi(n_0-1)d/\lambda_a \qquad (5.3)$$

since λ_a is usually very small compared to $n_0 d$, a small variation of n_0 or d produced by the exposing light can lead to a large phase change $\Delta\varphi$ of approximately π radians. We therefore set

$$\Delta\varphi = \Delta[2\pi(n_0-1)d/\lambda_a] = \pi \qquad (5.4)$$

For thin or plane holograms d approaches to λ_a. Since attainable values of index change Δn_0 are generally much less than n_0-1, we can in this case neglect the term containing Δn_0 then we are left with the condition

$$\Delta d \approx \lambda_a / 2(n_0 - 1) \qquad\qquad (5.5)$$

for maximum efficiency. Diffraction efficiency can be as high as 33.9% for sinusoidal gratings and 40.4% for square wave gratings. Examples of thin phase materials include photoconductor-thermoplastic films, etched photoresist films, photopolymers, and photographic emulsion bleached to have only surface relief.

5.4 Silver Halide Materials

Silver halide recording materials for holography are interesting for many reasons. Silver halide was the first material used for recording holograms; it is also the most important material for holography in respect of its numerous scientific and artistic applications. In addition, it has high sensitivity in comparison with many other alternative materials, it can be coated on both film and glass, it can cover even very large formats, it can record both amplitude and phase holograms, it has high resolving power, and is easily available. Nevertheless, it has some drawbacks; it is absorptive, it has inherent noise and limited linear response, it is irreversible, it needs wet processing, it creates printout problems in phase holograms, etc. Since silver halide materials are used in our experiments, these will be discussed in greater detail in next sections.

5.5 Non-Silver Materials

A detailed presentation of a wide range of recording materials for holography can be found in the book by Smith [49].

5.5.1 Dichromated Gelatin

Dichromated Gelatin (DCG) is a potential recording material for Lippmann type holograms. Dichromated gelatin has a high resolving power and remarkable brightness due to a refractive index modulation of 0.08, which is the largest among holographic materials known today. During the exposure of a dichromated gelatin emulsion to UV or blue light, the hexavalent chrominum ion (Cr^{6+}) is photoinduced to trivalent chrominum ion (Cr^{3+}) which causes cross-linking between neighbouring gelatin molecules. The areas exposed to light are hardened and become less soluble than the unexposed areas. Developing consist of a water wash which removes the residual or unreacted chemical compounds. Dehydration of swollen gelatin follows after the material has been immersed in isopropanol, which causes rapid shrinkage resulting in voids and cracks in the emulsion and thus creating a large refractive index modulation. The DCG material has rather low sensitivity of about $100mJ/cm^2$. The material is employed in the production of Holographic Optical Elements (HOE) mainly.

5.5.2 Photopolymer Materials

Photopolymer materials can be used for recording phase holograms. Normally, the materials have a short shelf-life and a rather limited refractive index change. Its sensitivity is not too bad though, and the advantages are a low noise level and its suitability for application of dry processing techniques.

A photopolymer recording material consists of three parts: A photopolymerisable monomer, an initiator system (initiates polymerisation upon exposure to light) and a polymer (the binder). First, an exposure is made to the information-carrying interference pattern. This exposure

polymerises a part of monomer. Monomer concentration gradients, formed by variation in the amount of polymerisation due to the variation in exposures, give rise to diffusion of monomer molecules from the regions of high concentration to the regions of lower concentration. The material is then exposed to regular light of uniform intensity until the remaining monomer is polymerised. A difference in the refractive index within the material is obtained. The sensitivity of these materials is about $10mJ/cm^2$.

5.5.3 Photoresist Materials

Photoresists are well known from electronic industry. In holography they are employed mainly for the production of master plates for embossed holograms and for manufacturing holographic gratings. A photoresist is a photosensitive material which produces a relief pattern in the material after its exposure and processing. The exposure to actinic radiation produces changes in the photoresist layer that result in solvency differentiation as a function of exposure. Processing is done with a suitable solvent dissolving either the unexposed or exposed regions, depending on whether the resist is of the negative or the positive type. The photoresist process can be used for making transmission holograms only. A typical photoresist for holography (e.g., Shipley AZ-1350) has a sensitivity of about $10mJ/cm^2$. It is sensitive for UV and for visible light up to 500nm.

5.5.4 Thermoplastic Materials

Thermoplastic recording materials for holography are found mainly in the non-destructive testing field. It has a multilayer structure consisting of a glass or Mylar substrate coated with a thin, transparent, conducting layer of indium oxide, a photoconductor, and a thermoplastic [57]. The film is initially

sensitised in darkness by applying a uniform electric charge to the top surface. On exposure and recharging, a spatially varying electrostatic field is created. The thermoplastic is then heated briefly, so that it becomes soft enough to be deformed by this field, and cooled to fix the variations in thickness.

The material's sensitivity is similar to that of the silver halide materials', its resolving power is quite high, and it requires only dry processing. The fast dry processing makes the material popular for the use in holographic cameras for non-destructive testing. The sensitivity is between 10 and 100 $\mu J/cm^2$ over the whole visible spectrum.

5.5.5 Ferroelectric Crystals

These normally rather small crystals of, e.g., lithium niobate ($LiNbO_3$) and barium titanate ($BaTiO_3$), are used mainly for scientific applications, e.g., phase conjugation and non-linear optical experiments. Holograms recorded in these materials consist of bulk space charge patterns. An interference pattern acting upon a crystal will generate a pattern of electronic charge carriers that are free to move. Carriers are moving to areas of low optical illumination where they get trapped. This effect will form pattern of net space charge, creating an electrical field pattern. As these crystals have strong electrooptical properties, the electrical field pattern will create a corresponding refractive index variation pattern, which means a phase hologram. These holograms can immediately be reconstructed with a laser beam different from the beams creating the hologram. The hologram can also be erased and a new hologram can be recorded in the crystal. The advantages of ferroelectric are their resolution, reversibility, instant readout, and rather high sensitivity.

5.6 Silver Halide Photographic Emulsion

Silver halide photographic emulsions are still most widely used recording materials for holography, mainly because of their relatively high sensitivity and because they are commercially available. In addition, they can be dye sensitised so that their spectral sensitivity matches the most commonly used laser wavelengths.

An apparent drawback of photographic material is that they need wet processing and drying; however, development is actually an amplification process, with a gain of the order of 10^6, which yields high sensitivity as well as a stable hologram. Another advantage of the formation of a latent image is that the optical properties of the recording medium do not change during the exposure, unlike materials in which the image is formed in real time. This makes it possible to record several holograms in the same photographic emulsion without any interaction between them.

Data on some of the commercial silver halide photographic emulsions available for holography are summarised in Table 5.1 and some characteristic curves for Agfa's material are given in Figure 5.1, 5.2, and 5.3.

Photographic emulsion primarily consists of extremely fine grains of silver halide compounds dispersed in gelatin. Also present in the gelatin are certain sensitising agents. The emulsion is coated over a transparent substrate which is either a glass plate or a flexible acetate film. For hologram recording with continuous wave laser, the rigid glass is preferred over the flexible film. Approximate thickness and intensity transmittance of some common emulsions are listed in Table 5.1.

When a two beam interference pattern exposes a photographic plate and the plate is developed, an absorption hologram is formed. During the development process the exposed silver halide grains are converted to

Table 5.1. Commercial holographic silver halide products

Material	Emulsion thickness (μm)	Spectral sensitivity (nm)	Sensitivity (μJ/cm^2) at				Resolving power (lp/mm)	Grain Size (nm)
			442	515	633	694		
Agfa								
8E75HD	7	<750	-	-	10	20	<5000	35/44
10E75	7	<750	-	-	1	2	<2800	90
8E56 HD	7	<560	25	-	-	-	<5000	35/44
Kodak								
649-F (plate)	17	<700	80	80	90	500	>2000	58
649-F (film)	6	<700	80	80	90	500	>2000	58
649-GH	6	<560	100	100	-	-	>2000	58
120	6	<700	50	40	40	40	>2500	50
125	6	<560	8	5	-	-	>1250	70
131	6	<700	5	3	0.5	100	>1250	70
SO-173	6	<700	50	-	40	40	>2500	50
SO-253	9	<700	5	3	0.5	100	>1250	70
SO-343	6	<560	100	100	-	-	>2000	58
HR-IA	6	<560	100	100	-	-	>2000	58
HR-TE	3	<560	300	200	-	-	>2000	58
Ilford								
FT340T (plate)	6	<700	-	-	200	-	<7000	30
Hotec R (film)	7	<700	-	-	20	50	<7000	30
SP695T (plate)	6	<560	200	100	-	-	<7000	30
SP672T (film)	7	<560	200	100	-	-	<7000	30
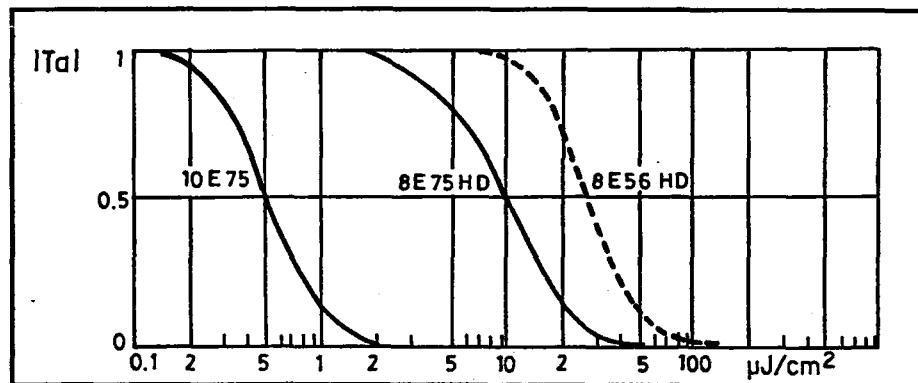
Figure 5.1 Curves of amplitude transmittance $|T_a|$ against log exposure for Agfa's photographic emulsion materials.

metallic silver. A bleach process may be used after development to convert the silver to a transparent compound; this in turn converts the absorption hologram to a phase hologram.
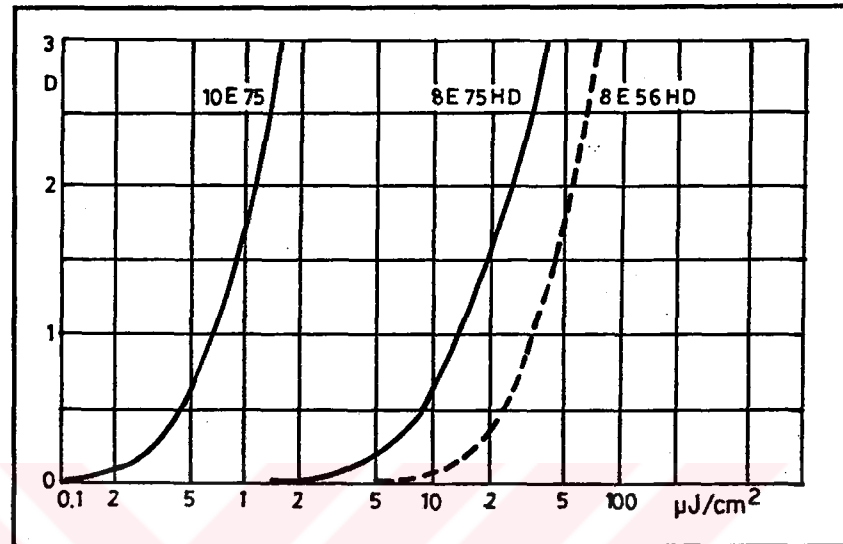
Figure 5.2. The characteristic curves for Agfa Holotest materials.
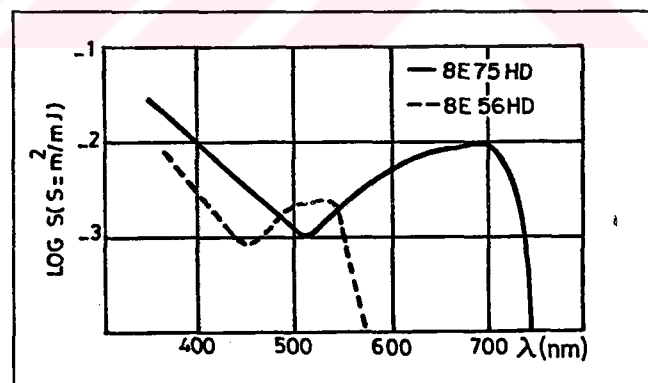
Figure 5.3. Absolute colour sensitivity curves for Agfa's materials. The curves indicate the exposure needed to obtain a density of 0,6 above fog.

5.7 Emulsion Shrinkage

The thickness of processed photographic emulsion layer is usually about 15 percent less than its original thickness, mainly because of the removal of the unexposed silver halide grains during fixing.

Because of this reduction in thickness, Λ' the fringe spacing in the hologram is less than Λ, the fringe spacing in the original interference pattern, except for special case when fringe planes are normal to the surface of the emulsion.

The effects of emulsion shrinkage are most noticeable in volume reflection holograms, since the fringe planes run almost parallel to the surface of the emulsion. When the hologram is illuminated with the white light, it reconstructs an image at a wavelength λ' which is given by the relation $\lambda'=(\Lambda'/\Lambda)\lambda$ where λ is the wavelength used to record the hologram. Typically, a reflection hologram recorded with a He-Ne laser ($\lambda=633nm$) reconstructs at a wavelength $\lambda' \approx 500nm$, giving a green image.

Because of emulsion shrinkage, amplitude holograms recorded in photographic emulsions also exhibit phase modulation which can modify the MTF. This phase modulation is mainly due to a surface relief structure arising from local tanning (hardening) of gelatin by the oxidation products of the developer in the immediate vicinity of the reduced silver.

After processing, the entire emulsion layer is swollen to more than five times its normal thickness and is very soft. The tanned gelatin in the vicinity of a clump of developed silver grains absorbs less water than the untanned areas and therefore dries more quickly. Shrinkage during drying pulls some of the gelatin from the adjacent untanned areas into the image areas, and, when the emulsion has dried, the higher density areas stand out

in relief because both the image silver and extra gelatin contribute to their bulk.

Since the relief image formed by local tanning is usually confined to low spatial frequencies ($<2000mm^{-1}$), it normally contributes very little to the reconstructed image. However, it can give rise to intermodulation noise. The formation of such a relief can be avoided by the use of a developer with a high sulphite content. Alternatively, the emulsion can be treated in a pre hardening bath before processing.

5.8 Modulation Transfer Function

The MTF curves for fine-grain photographic materials used for holography usually extend to quite high spatial frequencies. While the MTF can be measured with specially designed instruments it is derived most commonly in an indirect fashion from measurements of the diffraction efficiency of sinusoidal gratings with differential spatial frequencies recorded on these materials.

Typical curves of diffraction efficiency as a function of spatial frequency obtained for 8E75, 8E56, 10E75 and 10E56 emulsions for different wavelengths are presented in Figure 5.4. As can be seen, after an initial rapid drop, all them exhibit a gently sloping region covering the range of spatial frequencies used in holography. However, beyond a certain limit, the diffraction efficiency again decreases rapidly with increasing spatial frequency. These effects are more pronounced for the more sensitive emulsions (10E75 and 10E56) which have larger grains, and can be attributed to scattering in the virgin emulsion during the exposure.
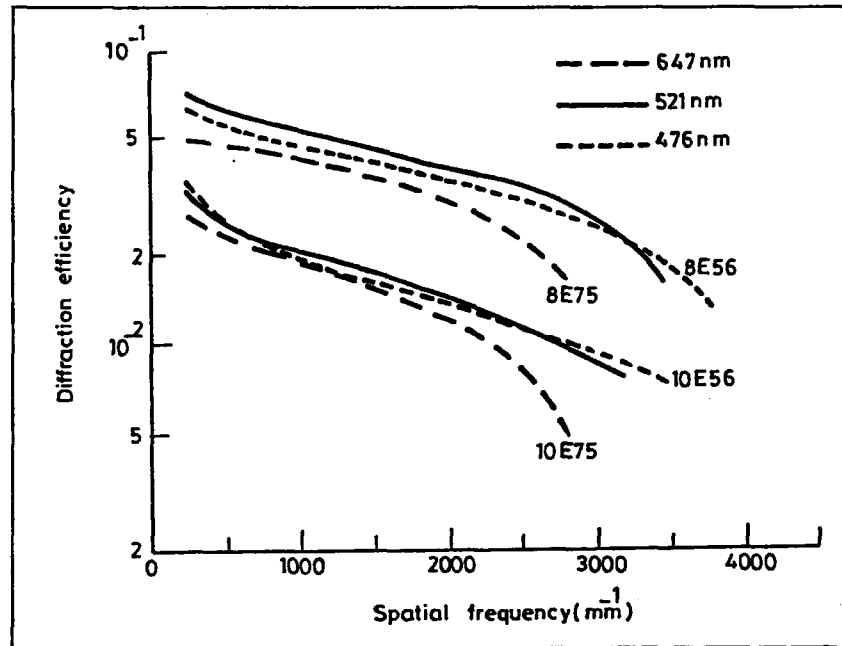
Figure 5.4. MTF curves of typical photographic emulsions used for holography.

5.9 Exposure and Sensitivity

One hologram recording material is considered more sensitive than another if, for fixed illumination conditions, less exposure is required to produce a hologram of specified diffraction efficiency.

If we assume that the light intensity averaged over an area containing many fringes is uniform over the hologram plate, the average exposure value E_0 is given by

$$E_0 = \eta_t \tau_e P/A \tag{5.6}$$

where η_t is the net power transfer efficiency from the laser to recording material, P is the output power of laser, τ_e is the exposure time, and A the cross-sectional area of the beam illuminating the hologram plate. In a typical hologram recording, only a fraction of the total laser output power that is usable actually exposes the hologram plate. If the subject is a diffuse reflector of light, then perhaps only 10% of the light incident on it will be received by the hologram plate. In addition there is approximately a 4% loss of light incident on each air-to-glass interface of the beam forming optics. Thus if we use above equation to calculate a limit to practical exposure, we should take η_t to be no more than 5%.

5.10 Film Processing Techniques

The term photographic film refers to an emulsion that is suspension of silver halide crystals in a protective colloid (usually gelatin)[12]. Photographic processes involve the interaction of light with certain of the silver halides. Generally for photographic purposes silver halides are considered to be either silver bromide, silver chloride, or silver iodine. When radiation falls on a photographic silver halide film, there is a tendency for a decomposing to occur. This decomposing reaction is quite complex but can be naively represented for silver bromide by the expression,

$$Ag^+ + Br^- + hv \rightarrow Ag + Br$$

This expression states that silver bromide crystals are made up of positive silver ions and negative bromide ions, and those silver halide crystals will decompose to metallic silver and bromide when light energy is added.

5.10.1 Developing

For practical purposes it is desirable to obtain a permanent image with a very little energy required to expose the film. The development process makes it possible to reduce the exposure time by over six orders of magnitude. When light falls on the silver halide in a photographic emulsion, it is reduced to extremely small particles of silver that form a latent image which is initially invisible. The latent image can be made visible by a photographic developer. A photographic developer is a reducing agent that acts as a catalytic centre for further reduction of silver halide crystals into silver. A good developer is one that selectively reduces exposed silver bromide crystals more rapidly than it reduces the unexposed crystals. The advantages or disadvantages of any particular developer lie in its ability to selectively reduce the exposed silver bromide and not the unexposed silver bromide. For any particular developer this selectivity will depend primarily on its temperature and alkalinity when used. The term alkali is meant to apply to those soluble metallic hydroxides that react with acids to form salts. The degree of alkalinity of a solution is determined by its pH. Values of pH above 7 are considered alkaline.

Some commonly used chemical compounds that have the required property of selective development of the exposed silver halide crystals are metol, phenidone, and hyroquinone. Combinations of these or other developing agents often improve the performance of the developer better than that of any developer used separately. Combining different developers together and varying the ratio of each usually will have a marked influence on the performance of the developer.

5.10.2 Accelerators

Most developing agents require an alkaline (high pH) solution before they can react to any great extent as a reducing agent. The presence and amount of an alkaline accelerator in the developing solution will determine the rate of development. Some commonly used accelerators are sodium hydroxide, borax, sodium bicarbonate, sodium carbonate, and sodium metaborate.

5.10.3 Buffering

A buffer is a solution composed of a combination of ingredients whose pH is unaffected by the addition of alkali or acids and acts as an accelerator to maintain uniform development activity. Some commonly used buffer combinations are; borax and boric acid, sodium hydroxide and boric acid, sodium carbonate and sodium bicarbonate, and sodium hydroxide and sodium phosphate.

5.10.4 Preservative

The developer being an oxidiser is itself oxidised not only when reducing the silver halide, but also when in contact with air. In order to slow down the oxidisation of developer when in contact with air a preservative (the most commonly used is sodium sulphite) is added. Sodium sulphite acts as a weak solvent for silver halide which in some types of developers tends to improve the grain and speed of the emulsion.

5.10.5 Restrainers

Restrainers are added to a developer to slow down the development process, usually to prevent the formation of fog. A strainer, most commonly used is potassium bromide, is usually added to prevent this fogging action from occurring.

5.10.6 Neutraliser (Short-Stop)

After development the film is placed in a solution to neutralise the alkalinity of the developer. Usually a solution of acetic acid is used rather that plain water to neutralise the alkali because the acid can rapidly neutralise any alkaline developer remaining in the emulsion gelatin. Acid bath also acts to dissolve or restrain the formation of calcium scum, preserve the acidity of fixing bath, and decrease the swelling of the gelatin emulsion.

5.10.7 Fixing

The metallic silver image formed during development in the emulsion is intermixed with undeveloped silver halide crystals. The undeveloped silver halide is still light sensitive and may still be reduced to metallic silver. For this reason the image is not permanent. In order to make the image permanent it is necessary to remove these undeveloped silver halide crystals from the emulsion. Generally sodium thiosulfate (hypo), ammonium thiosulfate are used to remove the undeveloped silver halide crystals from the gelatin emulsion by making them water soluble.

5.10.8 Hardeners

Hardeners are usually added to fixing solution to toughen the wet gelatin emulsion and make it resistant to abrasion. Hardeners are used to reduce the swelling of gelatin in water solution as well as to increase the temperature required for solution in water.

Potassium alum, chrome alum, or ammonium alum is usually added to the fixer to harden the photographic emulsions and to raise their melting point. Gelatin can also be hardened by heat, ultraviolet radiation, aluminium chloride, aluminium sulphate, or formaldehyde.

5.10.9 Rinsing

Rinsing of processed film is done to remove residual chemicals remaining in the emulsion that can cause staining; for example, residual hypo can cause silver sulphite to form, causing a brownish staining to form. The longer the rinse, the longer the film can be stored without staining.

Films are usually placed in a water-softening liquid to reduce the surface tension, such as calgon or photoflo, after rinsing is completed which prevents spotting caused by the rinse water collecting on the film in drops when drying.

5.10.10 Drying

Drying is relative since gelatins usually contain some water even when they are considered dry. Drying is usually accomplished by normal evaporation. It is also done sometimes by circulating clean dry air at room

temperature, or using an 80 percent alcohol rinse prior to drying to speed the process.

5.10.11 Bleaching

An absorption hologram recorded in a photographic emulsion can be converted into a phase hologram with a higher diffraction efficiency. The conversion involves a chemical bleaching of the emulsion. There are basically two kinds of bleach process. In one process the spatial variation of absorption constant is converted into corresponding thickness variation of the bleached emulsion. This thickness variation is also known as surface relief. In the second process the spatial variation of absorption constant is converted into a corresponding refractive index variation in the emulsion volume. A bleached hologram generally has both thickness and refractive index variations and is not absorptionless; its maximum diffraction efficiency is less than 70%.

5.11 Processing Chemicals

For creating phase holograms special developers and bleachers have been formulated to work in different processing regimes and with different materials. Developers and bleachers for reflection holograms are given below.

Developer GP 62 (reflection):
Solution A
Metol   15 g
Pyrogallol   7 g

Sodium sulphite	20 g
Potassium bromide	4 g
EDTA (sodium salt)	2 g
Water	1 L

Solution B

Sodium carbonate	60 g
Water	1 L

Mix 1 part A, 1 part B and 2 parts water. Develop for 2 min at 20°C.

Pyrochrome (van Renesse) developer (reflection):

Solution A:

Pyrogallol	10 g
Water	1 L

Solution B:

Sodium carbonate	60g
Water	1 L

Mix part A+B just before use., developing time 2 minutes at 20°C.

Rehalogenating bleach GP 432 (reflection, transmission):

Potassium bromide	50 g
Boric acid	1.5 g
Distilled water	1000 ml

Add p-benzoquinone 2g/l just before use, use undiluted.

Reversal bleaching, permanganate solution (reflection):

Potassium permanganate	3g
Sulphuric acid	10 ml
Water	1L

Kodak D19 developer (transmission):

Metol	2.2g
Hydoquinone	8g
Sodium sulphite (anhydrous)	90g
Sodium carbonate (anhydrous)	52.5g
Potassium bromide	5g
Water	1L

Use undiluted, developing time 4-5 minutes at 20°C.

CHAPTER VI

EXPERIMENTS

This chapter deals with the experimental procedures to investigate deformations, refractive index changes by using double exposure and difference holographic interferometry techniques.

6.1 Optical, Optoelectronic Elements and Light Sources

In all our experiments following optical and optoelectronic components are used:

- Spindler & Hoyer front surface plane mirrors, beam splitter plates, spatial filter and collimator.

- Scanning interferometer driver: Spectra Physics Model 588 J-Lok^{TM}.

- Interferometer analyser head: Spectra Physics Model 450-2.

- Power Meter: Coherent Radiation, Model 212.

- Intercavity etalon: Spectra Physics, Model 583 oven controlled etalon, with Model 482 temperature controller.

- Ar-ion laser: Spectra Physics, Model 2020-05.

During all experiments, stability of optical table was tested by constructing a Michelson interferometer system on the table. Basic set-up for Michelson interferometer is shown in Figure 6.1. In this set-up the beam from He-Ne laser is divided into two beams by the beam splitter BS. The partially

reflected beam from BS is directed to M1 and reflected through the beam splitter towards to lens L. The beam passing through BS is reflected back by the mirror M2. This reflected beam again reflected by BS towards lens L. When these two beams are expanded by the lens L and projected to a screen S a set of stable parallel fringes are observed. If optical table is not stable these fringes shift from dark to light. This shifting is in integral numbers of half wavelength. Our optical table is tested with this system and found to be stable during the experiments.
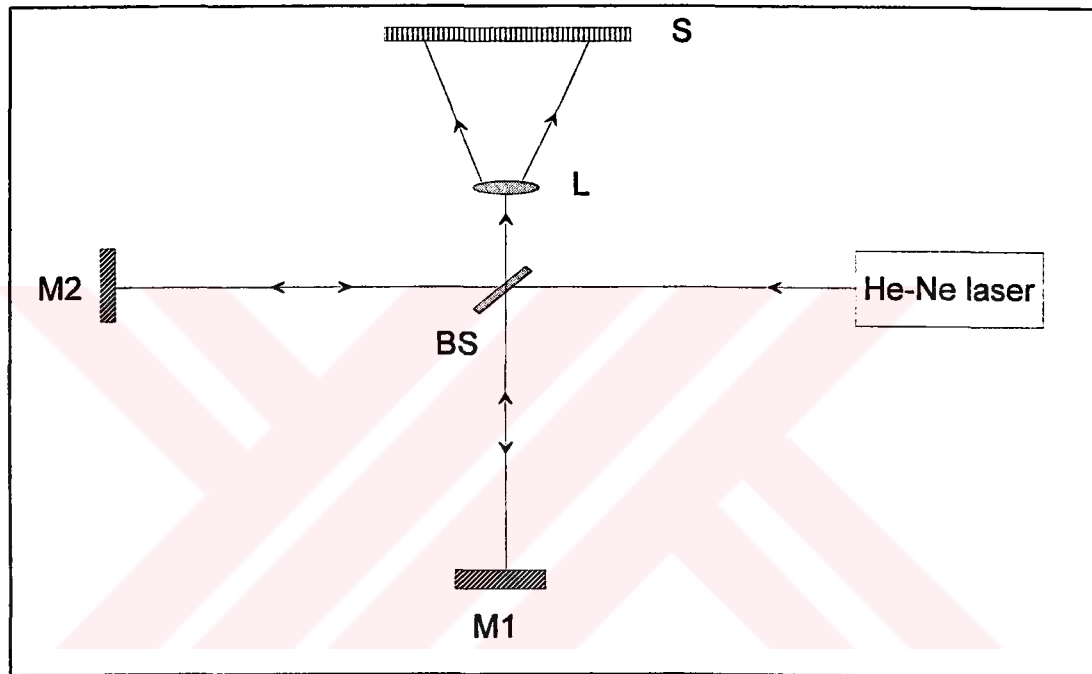
Figure 6.1. Set-up for stability testing (Michelson Interferometer)

As is well known, the coherent properties of the light source determine the visibility of the fringe pattern and consequently the quality of the recorded hologram. On the other side, the amount of the light scattered by the object on the recording plane is a function of its size and shape. The maximum area which can be viewed with a single hologram is governed basically by the amount of the laser power available. In this work the demand

74

on radiated power was a few watts at single frequency operation. To meet the power requirements and to obtain a high contrast interference we employed an argon ion laser equipped with a temperature controlled Fabry-Perot etalon (Spectra Physics Model 583). By means of this device a single mode operation was achieved that displayed a sufficient coherence length resulting in a good quality fringe pattern. Single mode operation is monitored on the oscilloscope using scanning interferometer system whose block diagram is shown in Figure 6.2.
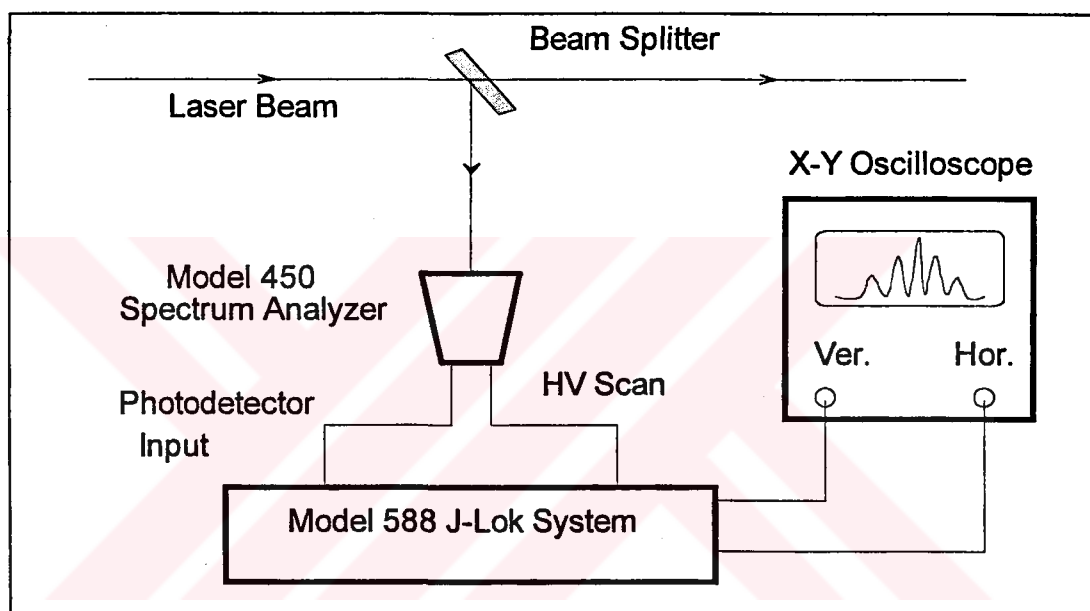

Figure 6.2. Block diagram of Scanning Interferometer.

6.2 Double Exposure Holography

In these experiments, two different set-ups are used to obtain double exposure holograms of transparent and diffusely reflective objects. An 220 V lamp was used as a transparent object and a surface of optical

mounting system, Coca Cola can, and ceramic resistors were used as a diffusely reflecting object.

The optical set-up used for double exposure holography of transparent object is shown in Figure 6.3. The set-up is similar to transmission holography set-up. The beam from Ar^+ laser is divided into two parts by beam splitter BS. The beam passing through BS is reflected by mirror M1 towards holographic plate HP. This beam is spatially filtered and collimated by Spindler&Hoyer spatial filter and collimator system which is not shown in the figure and serves for reference beam. The beam partially reflected by BS is expanded by a lens, which is not shown in the figure, passes through ground glass and object O (lamp), finally impinges on HP and serves for object beam.

The total power on HP is 2.5μW, which is measured by power meter (Coherent Radiation, Model 212) , with the beam ratio of approximately 1/4.

In the first exposure, no voltage is applied to lamp, and exposure time is 5 sec, which is found by trial error method for our experiments. After this exposure, 60 Vac is applied to the lamp and waiting about 2 minutes to have thermal equilibrium with surroundings, a second exposure is taken for 5 sec. This exposed holographic plate is then taken away from the holder, and processed with the procedures given below. Figure 6.4 shows the photograph of one of the holograms obtained in this set-up. As it can be seen from this photograph, fringes are due to refractive index change in the lamp.

The set-up used for double exposure holography of diffusely reflective object is shown in Figure 6.5. The beam from Ar^+ laser is divided into two by the beam splitter BS. The beam passing through the BS is reflected by M2 towards holographic plate HP. This beam is also spatially

76

filtered and collimated with the same system used in previous experiment. The partially reflected beam from BS is reflected by the mirror M1 towards
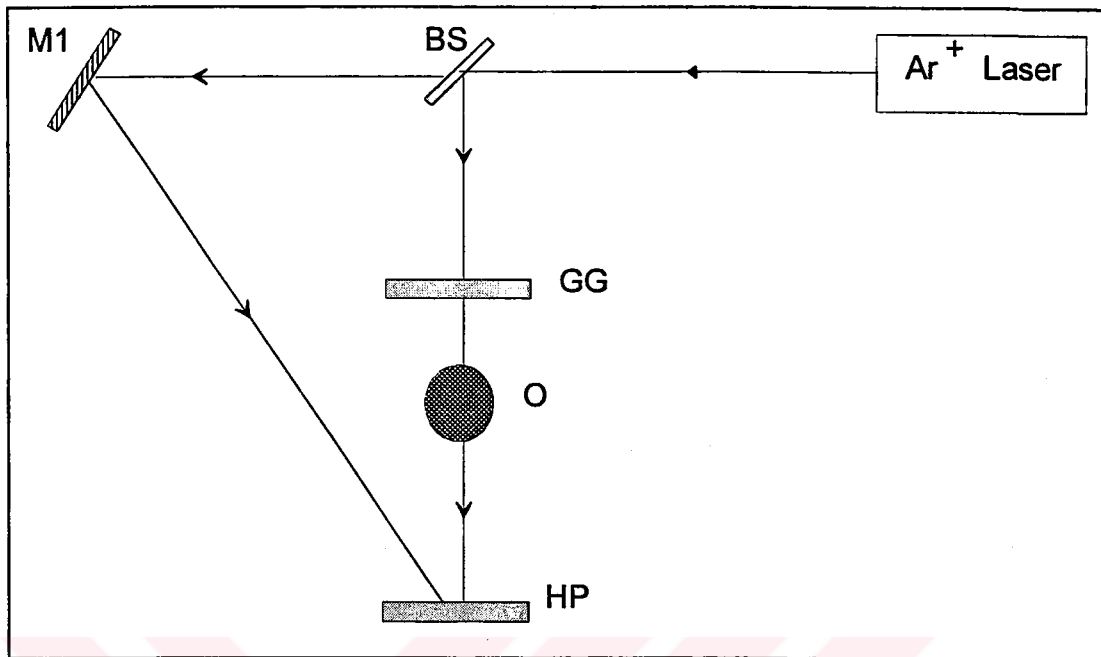

Figure 6.3. The set-up for double exposure hologram of transparent objects.

object O, which is a brass block, Figure 6.6, with adjusting screws. This beam is expanded by a lens which is not shown in the figure.

In the first exposure no mechanical load is applied to object. The beam ratio and total beam power on the HP are approximately 1/4 and 2.5 μW respectively. After exposing 5 sec, one of the screws is tightened a little bit in the middle of the object from the back side, and a second exposure of 5 sec is taken. The film is processed in the same manner as in the previous experiment.
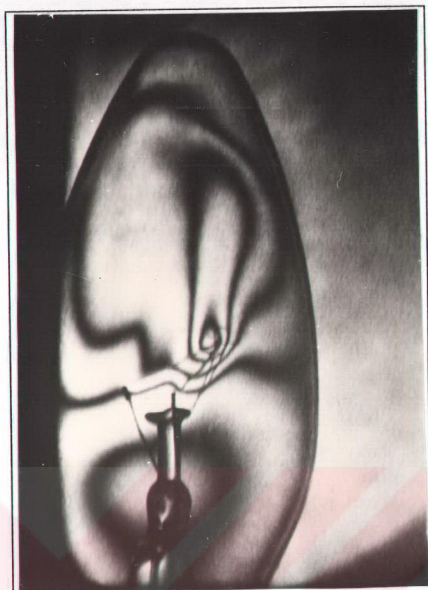
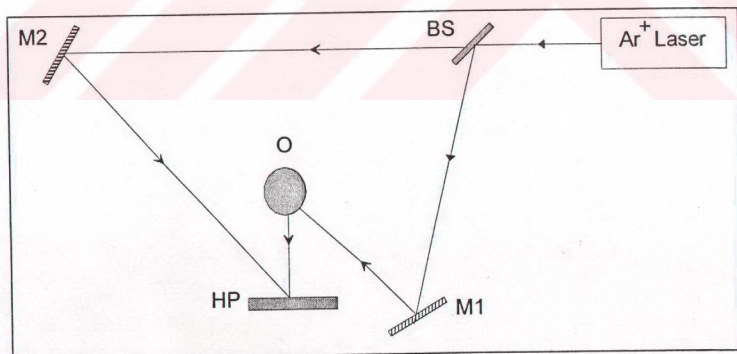Figure 6.4. Photograph of lamp hologram

Figure 6.5. The set-up for double exposure hologram of diffusely reflecting
objects.

Figure 6.6, shows the photograph of hologram taken by using this set-up. The fringes clearly show the displaced regions, which are due to applied force to the brass block. Figure 6.7 shows a Coco Cola can with a package rubber put on it. This hologram is obtained before the can is empty in the first exposure and half filled with water in the second exposure. The fringes clearly show the changes in the volume of the can. Figure 6.8 shows the two identical ceramic resistors connected in parallel in a circuit. This hologram is obtained with no current passing through the resistors in the first exposure and with 2 A DC current passing through the resistors in the second exposure. The fringes show the inhomogeneity in the ceramic resistors clearly in the same loading conditions.

Figure 6.6 Photograph of brass block hologram

Figure 6.7 Photograph of Coca Cola can hologram

Figure 6.8. Photograph resistor hologram

6.3 Difference Holography

The optical set-up used in the difference holography experiments is shown in Figure 6.9, where beam expanding elements are not shown. The laser beams illuminating the object and the holographic plate are expanded by diverging lenses. The arrangement is divided into two parts: the first part indicated by solid lines is used for recording master holograms while the second part (dotted lines) served for recording the difference interferometric fringe systems.

Laser beam from the argon-ion laser (Spectra Physics Model 2020-05) is divided into two parts. The beam passing through the beam splitters BS1, BS2, and BS3 and directed by the mirror M1 onto holographic plate HP serves as the reference beam for recording the master hologram. The beam reflected from the mirror M2 illuminates the master object O (solid lines).
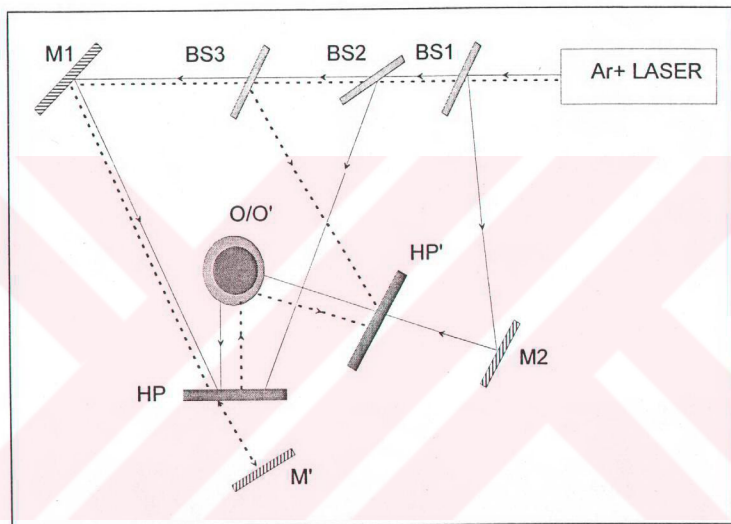
Figure 6.9. Set-up for difference holography

The object used as master as well as test object was a plate of brass mounted on a rigid body by three screws and a spring so that the surface of the plate to be investigated could be moved in three dimensions.

A double-exposure interferogram was made in the usual way by changing the position of the object surface between two exposures. Figure 6.10 shows a typical interferogram with small displacements produced by

this method. Then the developed hologram was placed in its original position accurately by means of the auxiliary beam coming from BS2. In the next step the master object O was replaced by the test object O', which was made by painting the object O by a spray paint to simulate the different but similar object. A new double-exposure interferogram concerning the object O' was recorded on the holographic plate HP' using the reference beam coming from the beam splitter BS3 and the object wave fronts reversed by the mirror M'. The position of the object from approximately the same initial value was changed to an arbitrary one. The holograms were developed in the usual processing technique described in section 6.4. As hologram recording material we used Agfa-Gevaert 8E56 HD NAH plates in thickness of 3.3 mm, whose holographic characteristics meet a considerable number of serious requirements for this specific application [49].

The interferometric fringes belonging to the master object, test object and their difference are shown in Figure 6.10, 6.11, 6.12 respectively.

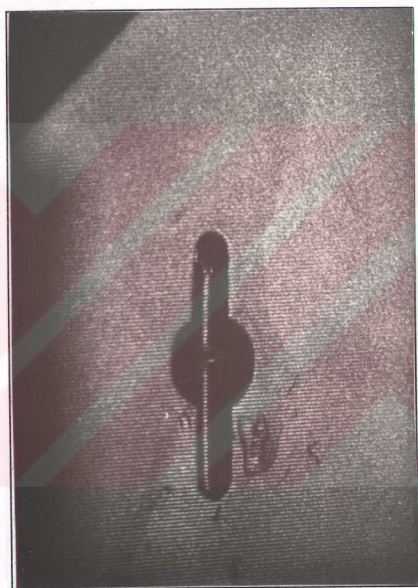Figure 6.10. Photograph of master hologram

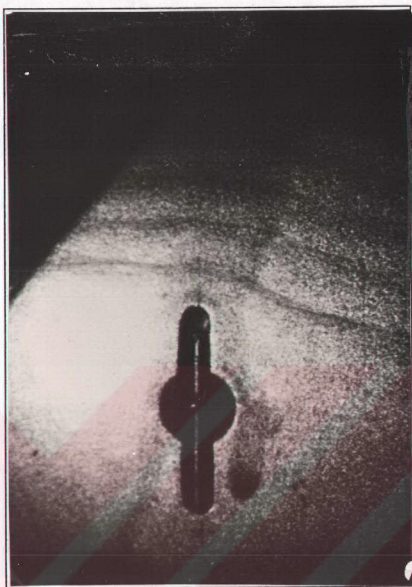Figure 6.11. Photograph of test hologram

Figure 6.12. Photograph of difference hologram

6.4 Chemical Processing of Films

Processing of exposed holographic plates

Develop 1 to 2 minutes until %10-20 dark by using D-19 solution

Rinse 3 minutes

Bleach until clear

Rinse 3 minutes

Photo Flo 5 sec

Dry

6.5 Obtaining Surface Relief Holograms on Agfa 8E56 HD Emulsion

The generation of a surface relief on a silver halide emulsion can have some applications in mass production, e.g., of HOE and display holograms. The embossing technique for mass replication of holograms utilises the transfer of a relief pattern. The demanding recording material for producing master holograms for embossing is the photoresist material. This material works very well but the disadvantage of having a rather low sensitivity and being only UV or blue sensitive, the powerful argon-ion lasers are required for the recording. The possibility of using other materials for masters for embossed holography is therefore of interest. A silver halide emulsion has the advantage of high sensitivity in any part of the visible spectrum. The large plates of embossing can therefore be produced with cheap low-power lasers, such as He-Ne laser.

The generation of a surface relief hologram is one way for obtaining transmission phase holograms already discussed in chapter 5. However, concerning silver-halide materials the effect is normally limited to low spatial frequencies. Also sometimes an unwanted surface-relief pattern is created as a result of certain bleaching processes. Such a pattern is then only considered a source of noise.

Altman [58] used Kodak 649-F emulsion, which is a thick and rather hard emulsion, for producing pure relief images. After development (Kodak HRP developer), the plate was bleached in Kodak R-9 bleach. A surface relief of about $1\mu m$ was observed when the emulsion was exposed to an optical density of 4.

This was confirmed by Cathey [58] who measured the emulsion surface-profile using Taylor Hobson Taylsurf. Gratings with different spatial frequencies recorded on Kodak 649-F plates were investigated. He found

that at 65 l/mm the height of fringes varied from 30 nm to 140 nm by increased exposure. At 275 l/mm, the depth was only 10 nm. Similar measurements were made by Hannes [59].

The papers describing improved surface-relief holograms continued to appear in [59-61]. Naturally, much of the Russian work has been carried out on ultra-fine-grained emulsions, such as PE-2 material. They also found a dependence of the height of surface relief on the spatial frequency, which was explained in the following way; in gelatin there is a competition between the intermolecular attractive forces, generated by drying, and surface tension forces. When the spatial frequency of relief structure becomes higher, the curvature of the gelatin surface becomes larger, which means increased surface-tension forces which create a reduced height of the surface relief.

Galpern et. al., [62] investigated various processing methods. Their investigations confirmed the earlier findings that nonhardening development followed by hardening bleaching produced the highest relief images for spatial frequencies 1080 and 1340 l/mm. Their developer composition is;

Relief Developer:

Metol	4g
Hyroquinone	8g
Ascorbic acid	26g
Sodium carbonate	40g
Potassium thiocyanate	4g
Ammonium bromide	2g
Water	1L

Concerning the hardening bleach, the best results are obtained with standard Kodak R-10 bleach. The surface-relief processing steps are the following

    1- Preheat the unexposed material for 1 hour at 90°C

    2- Expose the plate to obtain a high density

    3- Develop in relief developer

    4- Wash

    5- Bleach in Kodak R-10 until clear

    6- Soak in ammonium dichromate solution 5g/l for 5 minute

    7- Dip a sulphuric acid solution of pH 3

    8- Wash in water at 20°C

    9- Dry at an elevated temperature of 70°C

Using this procedure it was possible to obtain about 30% diffraction efficiency of aluminised gratings recorded on PE-2 at 1080 l/mm and 20% at 1340 l/mm.

        In this work, we tested above relief developer on Agfa 8E56 HD emulsions. For this reason we constructed a simple set-up to obtain a grating hologram.
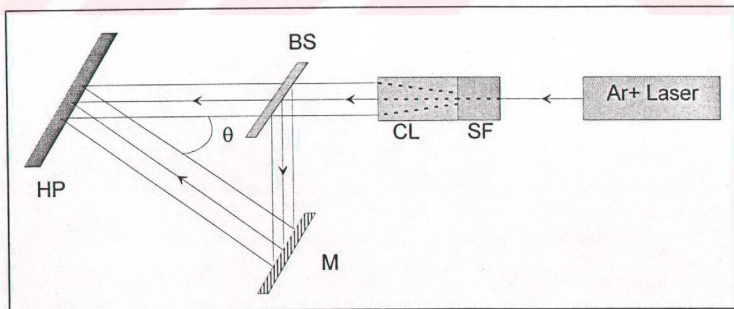

Figure 6.13. The simple set-up for producing diffraction grating.

In Figure 6.13., argon-ion laser beam (514.5 nm) is spatially filtered and collimated by SF and CL respectively. This beam is divided into two by the beam splitter BS. The beam passing BS and the beam reflected by the mirror M interfere on the holographic plate HP (Agfa 8E56 HD). The beam ratio is about 1. The angle, θ, between the interfering beams is about 28° and 52°. The spacing between interference fringes is given by

$$d = \frac{\lambda}{2\,sin\left(\dfrac{\theta}{2}\right)}$$

where λ is the recording wavelength, in our case it is 514.5 nm, and θ is the angle between the two interfering beams. At different exposure rates and at two different angles of interference a set of grating holograms are recorded. The processing of films are made by using the surface developer. The Kodak R-10 bleach is as follows;

Solution A:

Ammonium dichromate	20g	
Sulphuric acid (conc.)	14 ml	
Water	1L	

Solution B:

Potassium bromide	92g	
Water	1L	

Mix 1 unit A + 1 unit B + 10 units water before use.

6.6 Imaging the Profile of Gratings

The surface profile of gratings produced by the surface relief processing are scanned by an atomic force microscope (TopoMetrix, TMX 2000) in contact mode. This system consists of the following subsystems:

computer (CPU), electronic control unit (ECU), printer, microscope stage, and video monitor. The computer hardware and software consist of :

- Computer: PC compatible, 80486
- Monitor: Multisync colour and video monitor
- RAM: Minimum 8 Megabyte
- DSP: Spectrum 32 bit, 33 MHz
- Tape drive: 240 Megabyte streaming tape
- Graphics board: Hercules Dynamite Pro
- Hard Drive: Minimum 25 Megabyte free space
- Mouse: 2-button
- Microsoft Windows™ 3.1 or greater.
- TopMetrix SPM V3.0 Software.

This system has the scan range of 150X150x10 μm. The larger the scan range, lower is the achievable resolution. As an example, a scanner with 2 micron vertical dynamic range will have a vertical resolution of 0.1 angstrom and a scanner with 7 microns dynamic range will have a resolution of 0.7 angstrom.

The images of profiles are shown, after making a levelling operation on the images, in Figures 6.14, 6.15, 6.16. Figure 6.14 shows the grating profile which is produced at the angle $\theta \approx 52°$ and at 50 μJ/cm². This figure reveals that some profile is formed on gelatin surface. The profile of the grating obtained at 200μJ/cm² with the angle $\theta \approx 28°$ is shown in Figure 6.15. In this figure, profile of fringes are clearly seen, even height of the relief is large. To test the virgin emulsion, one of the films is exposed directly to laser light, homogenous intensity distribution, at 100 μJ/cm². and the same developing and bleaching processes are used. Image of the virgin emulsion is shown in Figure 6.16. To see the spatial distribution of relief structures on the emulsions 1-D FFT (on x-axis) operation is made on the images of Figure

6.14- 6.16. Power spectrum of the images are shown in Figures 6.17-6.19 respectively. From these figures it can easily be seen that, there are some noisy structures on the emulsion.

Figure 6.14. The profile of grating obtained by AFM, grating parameters are $\theta \approx 52°$ at $50\mu J/cm^2$.
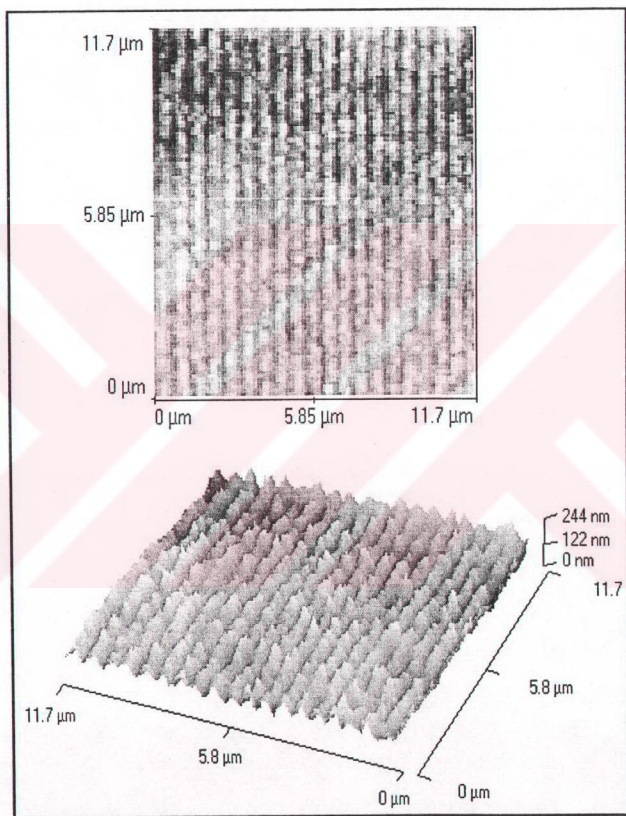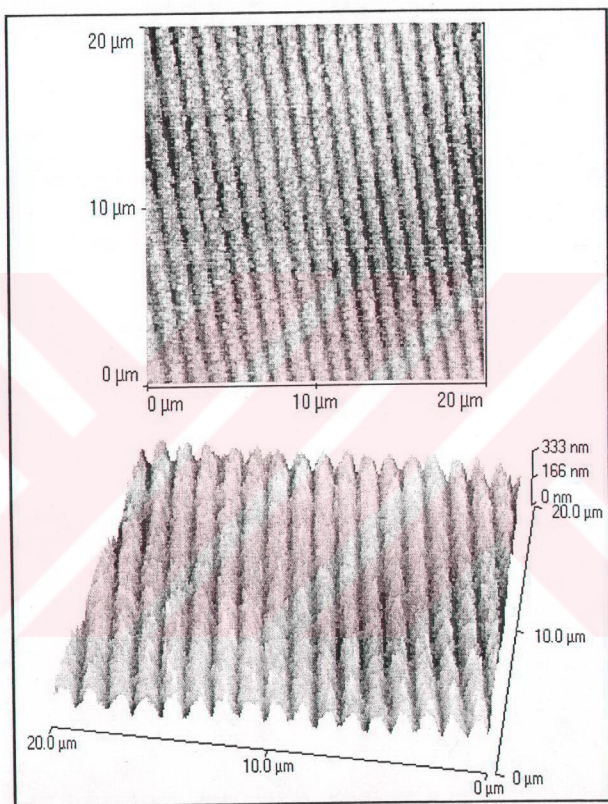
Figure 6.15. The profile of grating obtained by AFM, grating parameters are
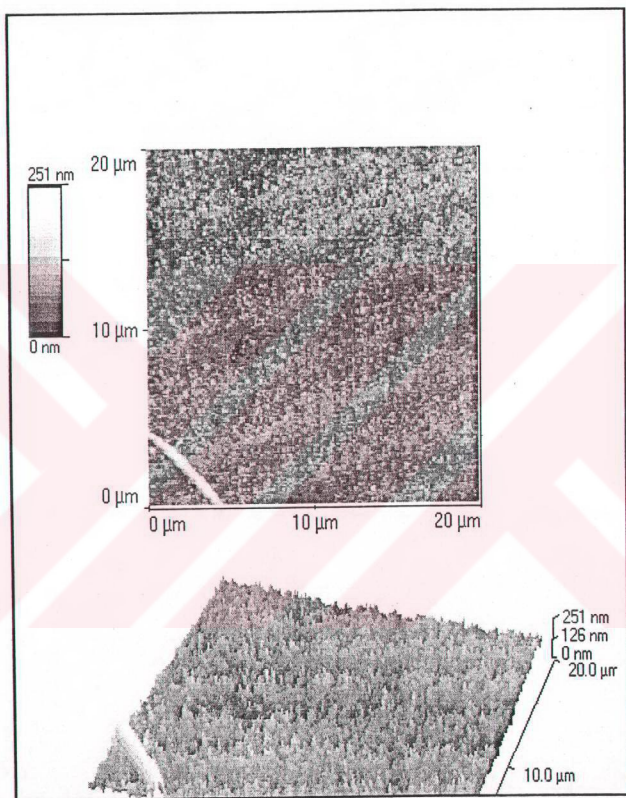$\theta \approx 28°$ at $200\mu J/cm^2$.

Figure 6.16. The profile of processed photographic emulsion obtained by
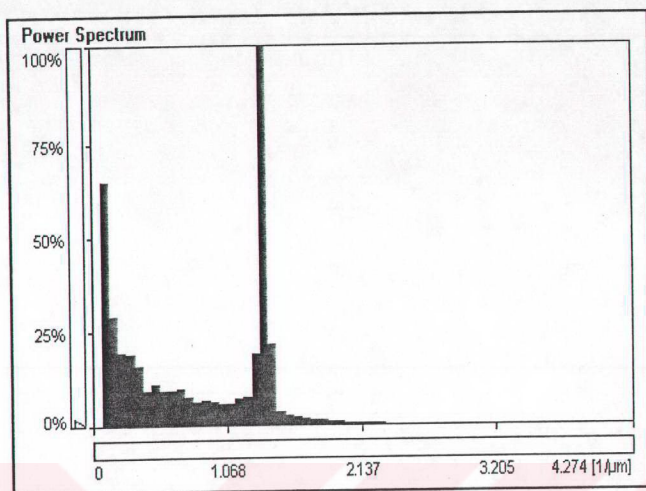AFM, exposed to 50 $\mu J/cm^2$.

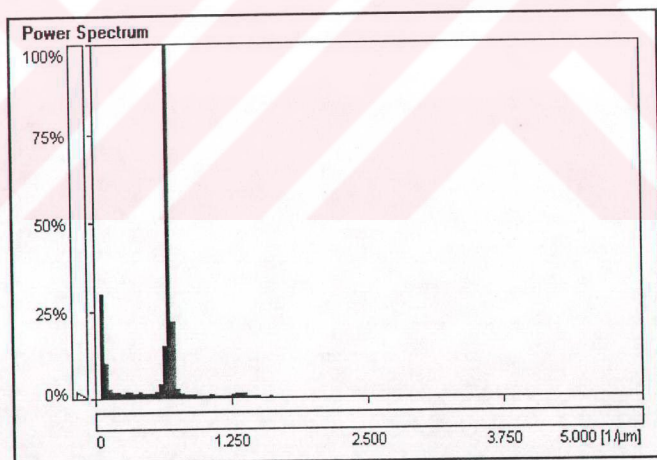Figure 6.17. Power spectrum of Figure 6.14 on x-axis

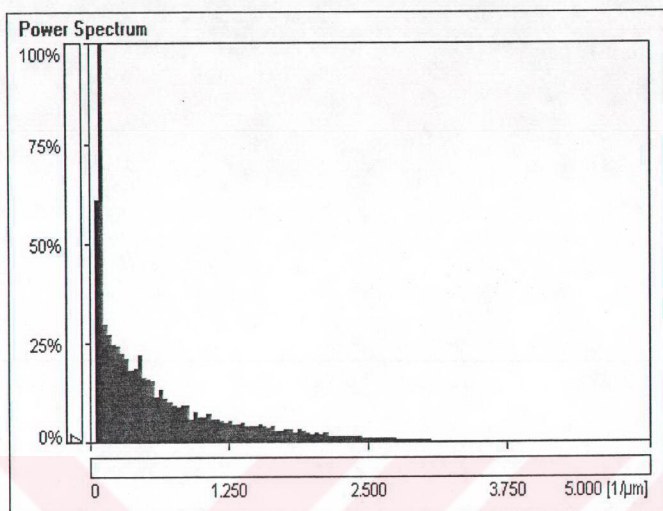Figure 6.18. Power spectrum of Figure 6.15 on x-axis

Figure 6.19. Power spectrum of Figure 6.16 on x-axis.

CHAPTER VII

CONCLUSION

The usual holographic interferometric techniques offer the possibility for deformation and shape measurements of objects but do not allow their comparison in direct interferometric way. To compare them, the interferograms of the individual objects are to be evaluated and only then can be calculated date be compared numerically. DHI makes the direct holographic interferometric comparison possible by using a special kind of object illumination in the usual holographic interferometric techniques.

There are two main advantages of direct comparison possibly offered by DHI. First, it is relatively fast. The difference is produced in a purely optical way and the computer aided evaluation of individual interferograms is not needed. It is especially important if the difference has to be evaluated only qualitatively. Second, the practical range of measurements is extended. DHI works even if the fringe systems of the objects to compared are too dense in themselves to be observed without high magnification, but are not washed out by the speckle phenomenon. High magnification restricts the field of view and the fringe system can be observed in small parts only. This advantage is especially important in the comparison of the shape of objects of rapidly altering forms with high sensitivity.

In this work, implementation of double exposure holography and difference holographic interferometry on some simple objects are

demonstrated. Double exposure holography is a simple technique that can be used a non-destructive technique which can be applied to visualise displacements, deformations and changes in refractive index in precision of wavelength of light used in recording the holograms as shown in Figures 6.4, 6.6-6.8.

As difference holographic interferometry technique, as an extension of double exposure holography, can show the differences of two different but macroscopically similar objects interferometrically this method is used in our work. The results of the work shown in Figure 6.10-12 directly show differences of two similar objects under the same load conditions.

It is important to note that the replacement of the objects need not be performed on the same place with interferometric precision. Because of the positioning accuracy which can be deformation or shape will be compared not in the proper points. The inaccuracy which can be tolerated depends upon the rapidity of the change of deformation or shape along the individual object surfaces. If this change is slow the inaccuracy can be quite large.

The advantages mentioned above make DHI useful not only in the laboratory research and development but presumably even in the industry as, for instance, a controlling unit in a assembly line. In the case of deformation measurement, its promptness is limited because a deformation has to be performed between the two exposures. The exposure time is a limiting factor as well but it can shortened by improving the quality of the hologram used for illumination and by using high power lasers. The stability required is also proportional with the duration of the measurement.

The use of thermoplastic film or other fast recording material can reduce development time considerably. However, it must remembered that

holograms of good quality can not be made of every object. The objects of diffuse surfaces are preferred and products manufactured to a high precision usually do not fall in this category.

Another development which attracted considerable attention has been the marriage between holographic interferometry and phase-shifting techniques. The integration of the two processes has led to a significant enhancement of the potentialities of holographic interferometry in non-destructive testing and in the measurement of deformations and shapes of diffuse objects quantitatively. Therefore, to make quantitative measurements digital and optoelectronic methods should be used in future works. For this reason one needs high resolution CCD camera, a dedicated computer system to record the hologram, process the images and show the result on the computer screen directly.

In this work, it also has been demonstrated how to obtain relief hologram structures on Agfa 8E56 HD photographic emulsion. It can bee seen in the Figures 6.14-15 that it is possible to obtain relief structures on these films by using the relief developer, but processing techniques and chemicals should be optimised to obtain noise free, high spatial frequency structures and large relief depths on this type emulsion. The single diagonal line on the lower left of the Figure 6.16 is intentionally made by directly passing the film across the laser beam. It can be concluded from these images and power spectrums that if the exposure high, the noise in the image decreases considerably and obtainable relief height decreases at high spatial frequencies due to surface tension on the gelatin surface and relief height increases if the exposure increases.

REFERENCES

[1]   Gabor D., Microscopy by reconstructed wave-fronts, *Proc. Roy. Soc. (London)*, **A197**(1949), 454-487

[2]   Gabor D., Microscopy by reconstructed wave-fronts II, *Proc. Phys. Soc.*, (London), **B64**(1951), 449-469

[3]   Leith E.N., UpatnieksJ., Reconstructed wavefronts and communication theory, *J. Opt. Soc. Am.*, **52**(1962), 1123-1130

[4]   Denisyuk Y. N., On the reproduction of the optical properties of an object by the wave field of its scattered radiation, *Opt. Spektrosk.*,**15**(1963), 522-532

[5]   van Heerden P. J., Theory of optical information storage in solids, *Appl. Opt.*, **2**(1963), 393-400

[6]   Powell R. L., Stetson K. A., Interferometric vibration analysis by wavefront reconstruction, *J. Opt. Soc. Am.*, **55**(1965), 1593-1598

[7]   Burch J. M., The application of lasers in production engineering, *Prod. Eng.*, **44**(1965), 431-443

[8]   Brooks R. E., Heflinger L. O., Wuerker R. F., Interferometry with a holographically reconstructed comparision beam, *Appl. Phys. Lett.*, **7**(1965), 248-249

[9]   Haines K. A., Hildebrand B. P., *Appl. Opt.*, **5**(1966), 595

[10]   Vest C.M., Holographic Interferometry, Interscience, New York, 1979

[11]   Ostrovsky Y.U., Butusov M.M, Ostrovskaya G.V., Interferometry by Holography, Springer Series in Optical Sciences Vol 20, Springer-Verlag, Berlin, Heidelberg, 1980

[12]   Ostrovsky Y. I., Schepinov V. P., Yakolev V. V., Holographic Interferometry in Experimental Mechanics., Springer Series, Optical Sciences Vol. 60, Springer-Verlag, Berlin, Heidelberg, 1991

[13]   Schumann W., Dubas M., Holographic Interferometry, Springer Series Optical Sciences Vol. 16, Springer-Verlag, Berlin, Heidelberg, 1979

[14] Schumann W., Zurcher J. P., Cuche D., Holography and Deformation Analysis, Optical Sciences Vol. 46, Springer-Verlag, Berlin, Heidelberg, 1985

[15] Rastogi P. K. (ed.), Holographic Interferometry- Principles and Methods, Springer Series in Optical Sciences Vol 68, Springer-Verlag, Berlin, Heidelberg, 1994

[16] Rao M.V., Samuel R., Nair P.S., Applications of Holographic Interferometry for Spacecraft Structural Components, *Opt. Eng.*, **33**(1994), 1876-1880

[17] Lefaucheux F., Robert M.C., Bernard Y., Gits S., Nucleation and Growth of Some Solution-Grown Crystals in Gel Media Visualization by Interferometric Holography, *Crystal Research and Technology*, **19**(1984), 1541-1547

[18] Bedarida F., Boccacci P., Aquilano D., Zefiro L., Vaccari G., Rubbo M.,Sgualdino G., Mantovani G., Growth of Sucrose Crystals and Tapering Effect Studied by Holographic Interferometry, *Journal of Crystal Growth*, **89**(1988), 395-404

[19 Spatz T.L., Poulikakos D., Holographic Interferometry Experiments on the Growth of Ice from a Horizontal Pipe, *International Journal of Heat and Mass Transfer*, **34**(1991), 1847-1859

[20] Chen W.C., Shen Y.X., Ma W.Y., Li M., Chen Y.S., In Situ Observation of Kb5 Crystal Growth Under Purely Diffusion Gel Systems by Holographic Interferometry, *Chinese Physics Letters*, **8**(1991), 469-471

[21] Silvennoinen R., Nygren K., Rouvinen J., Petrova V., Bone Structure Studies with Holographic Interferometric Nondestructive Testing and X-Ray-Methods, *Opt. Eng.*, 33(1994), 473-478

[22] Dermaut L.R., Vandenbulcke M.M., Evaluation of Intrusive Mechanics of the Type Segmented Arch on a Macerated Human Skull Using the Laser Reflection Technique and Holographic-Interferometry, *American Journal of Orthodontics and Dentofacial Orthopedics*, **89**(1986), 251-263

[23] Ferre J.C., Chauveaux D., Barbin J.Y., Holographic Interferometry in the Biomechanical Study of Femoral Behavior, with and Without Prosthesis, *Surgical and Radiologic Anatomy*, **12**(1990), 273-279

[24] Rastogi P.K., Pflug L., Jacquot P., Holographic-Interferometry Applied at Subfreezing Temperatures - Study of Damage in Concrete Exposed to Frost Action, *Opt. Eng*, **27**(1988), 172-178

[25] Park D.W., Jung J.O., Application of Holographic-Interferometry to the Study of Time-Dependent Behavior of Rock and Coal, *Rock Mechanics and Rock Engineering*, **21**(1988), 259-270

[26] Rastogi P.K., Pflug L., Jacquot P., Holographic Interferometry Applied to the Study of Frost Damage in Concrete, *Journal of Physics E Scientific Instruments*, **20**(1987), 1522-1525

[27] Miller R.A., Shah S.P., Bjelkhagen H.I., Crack Profiles in Mortar Measured by Holographic Interferometry, *Experimental Mechanics*, **28**(1988), 388-394

[28] Mobasher B., Castromontero A., Shah S.P., A Study of Fracture in Fiber Reinforced Cement Based Composites Using Laser Holographic Interferometry, *Experimental Mechanics*, **30**(1990), 286-294

[29] Anson M., Chung S.H., Pinder A.C., Keating M.J., Acoustic Vibration of the Amphibian Eardrum Studied by White Noise Analysis and Holographic Interferometry, *J. of the Acoustical Soc. of Am*, **78**(1985), 916-923

[30] Vandenbulcke M.M., Burstone C.J., Dermaut L.R., Sachdeva R.C.L., The Center of Resistance of Anterior Teeth During Intrusion Using the Laser Reflection Technique and Holographic-Interferometry, *American Journal of Orthodontics and Dentofacial Orthopedics*, **90**(1986), 211-220

[31] Rastogi P.K., Comparative Holographic-Interferometry - A Nondestructive Inspection System for Detection of Flaws, *Experimental Mechanics*, **25**(1985), 325-337

[32] Ostsemin A.A., Sitnikov L.L., Shakhmatov M.V., Erofeev V.V., Deniskin S.A., Determination of the Stress Intensity Coefficients for an Oblique Crack by the Method of Holographic Interferometry, *Industrial Laboratory USSR*, **53**(1987), 1190-1193

[33] Bryanstoncross P.J., The Use of Holographic-Interferometry to Visualize the Trailing Edge Flow Structure at the Wheel Exit of a Turbocharger, *Journal of Photographic Science*, **34**(1986), 77-80

[34] Lee T., Fisher M., Schwarz W.H., The Measurement of Flow Induced Surface Displacement on a Compliant Surface by Optical Holographic Interferometry, *Experiments in Fluids*, **14**(1993), 159-168

[35] Williams J.E., Peterson R.W., The Application of Holographic Interferometry to the Visualization of Flow and Temperature Profiles in a MOCVD Reactor Cell, *Journal of Crystal Growth*, **77**(1986), 128-135

[36] Nelson D., Fuchs E., Makino A., Williams D., Residual Stress Determination by Single-Axis Holographic Interferometry and Hole Drilling .2. Experiments, *Experimental Mechanics*, **34**(1994), 79-88

[37] Thalmann R., Dandliker R., Strain-Measurement by Heterodyne Holographic Interferometry, *Appl. Opt.*, **26**(1987), 1964-1971

[38] Kaufmann G.H., Vest C.M., Thermal Waves Visualized by Holographic Interferometry, *Appl. Opt.*, **26**(1987), 2799-2803

[39] Wakimoto T., Otsuka A., Application of Laser Hologram Interferometry to the Distortion Determination of Sugar-Coated Tablets, *Drug Development and Industrial Pharmacy*, **12**(1986), 641-650

[40] Phillips L.C., Kelly R.G., Moran P.J., Wagner J.W., An Investigation of the Volume Change Associated with Discharge of Lithium Iodine Batteries via Holographic Interferometric Techniques, *Journal of Electrochemical Society*, **133**(1986), 1-5

[41] Kussmaul K., Ettemeyer A., Deformation Analysis of a 900 MW Reactor Pressure-Vessel Head by Means of Holographic Interferometry, *Nuclear Engineering and Design*, **102**(1987), 307-312

[42] Ratnam M.M., Evans W.T., Comparison of Measurement of Piston Deformation Using Holographic Interferometry and Finite Elements, *Experimental Mechanics*, **33**(1993), 336-342

[43] Habib K., Initiation of Stress Corrosion Cracking of Ti90-Al6-V4 Wire in Aqueous Solution - Nondestructive Monitoring by Holographic Interferometry, *Optics and Laser in Engineering*, **20**(1994), 81-85

[44] Reuss D.L., Schultz P.H., Interferometric Temperature Measurements of a Flame in a Cylindrical Tube Using Holography, *Appl. Opt.*, **26**(1987), 1661-1667

[45] Geniatulin A.M., Investigation of Composite Cutting Tools by Holographic Interferometry, *Soviet Engineering Research*, **7**(1987), 70-73

[46] Kasprzak H., Sultanova N., Simple Holographic Interferometric Method of Investigating the Poisson Coefficient and Elasticity Moduli, *Opt. Eng.*, **33**(1994), 194-197

[47] Tentori D., Homogeneity Testing of Optical Glass by Holographic Interferometry, *Appl. Opt.*, **30**(1991), 752-755

[48] Harriharan P., Optical Holography, Cambridge University Press, 1984

[49] Smith H.M, Holographic Recording Materials, Topics in Applied Physics Vol 20, Springer-Verlag, Berlin Heidelberg, New York, 1977

[50] Collier R. ., Burckhardt C. B., Lin L. H., Optical Holography, Academic Press, New York, 1971

[51] Kogelnik H., Coupled wave theory for thick hologram gratings, *Bell. Sys. Tech. J.*, **48**(1968), 2909-2947

[52] Gyimesi F., Fuzessy Z., Difference Holographic Interferometry - Theory, *J.of Modern Optics*, **35**(1988), 1699-1716

[53] Fuzessy Z., Gyimesi F. , Difference Holographic Interferometry Displacement measurement, *Opt. Eng.*, **23**(1984), 780-783

[54] Fuzessy Z., Gyimesi F., Banysz I., Difference Holographic Interferometry (DHI): Single Reference Beam Technique, *Optics. Comm.*, **68**(1988), 404-407

[55] TopoMetrix, TMX 2000 Discoverer Scanning Probe Microscope User's Manual, Version 3.0X.

[56] Bennet J.M., Jahamir J., Podlesny J.C., Balter T.L., Hobbs D.T., Scanning Force Microscope as a Tool for Studying Optical Surfaces, *Appl. Opt.*, **34**(1995), 213-230

[57] Lin L.H., Beauchamp H. L., *Appl. Opt.*, **9**(1970), 2088-2092

[58] Altman J.H., Pure relief images on type 649-F plates, *Appl. Opt.*, **5**(1966), 1689-1690.

[58] Cathey W.T., Spatial phase modulation of wavefronts in spatial filtering and holography, *J. Soc. Opt. Am.*, **56**(1966), 1167-1171

[45] Geniatulin A.M., Investigation of Composite Cutting Tools by Holographic Interferometry, *Soviet Engineering Research*, **7**(1987), 70-73

[46] Kasprzak H., Sultanova N., Simple Holographic Interferometric Method of Investigating the Poisson Coefficient and Elasticity Moduli, *Opt. Eng.*, **33**(1994), 194-197

[47] Tentori D., Homogeneity Testing of Optical Glass by Holographic Interferometry, *Appl. Opt.*, **30**(1991), 752-755

[48] Harriharan P., Optical Holography, Cambridge University Press, 1984

[49] Smith H.M, Holographic Recording Materials, Topics in Applied Physics Vol 20, Springer-Verlag, Berlin Heidelberg, New York, 1977

[50] Collier R. ., Burckhardt C. B., Lin L. H., Optical Holography, Academic Press, New York, 1971

[51] Kogelnik H., Coupled wave theory for thick hologram gratings, *Bell. Sys. Tech. J.*, **48**(1968), 2909-2947

[52] Gyimesi F., Fuzessy Z., Difference Holographic Interferometry - Theory, *J.of Modern Optics*, **35**(1988), 1699-1716

[53] Fuzessy Z., Gyimesi F. , Difference Holographic Interferometry Displacement measurement, *Opt. Eng.*, **23**(1984), 780-783

[54] Fuzessy Z., Gyimesi F., Banysz I., Difference Holographic Interferometry (DHI): Single Reference Beam Technique, *Optics. Comm.*, **68**(1988), 404-407.

[55] TopoMetrix, TMX 2000 Discoverer Scanning Probe Microscope User's Manual, Version 3.0X.

[56] Bennet J.M., Jahamir J., Podlesny J.C., Balter T.L., Hobbs D.T., Scanning Force Microscope as a Tool for Studying Optical Surfaces, *Appl. Opt.*, **34**(1995), 213-230

[57] Lin L.H., Beauchamp H. L., *Appl. Opt.*, **9**(1970), 2088-2092

[58] Altman J.H., Pure relief images on type 649-F plates, *Appl. Opt.*, **5**(1966), 1689-1690.

[58] Cathey W.T., Spatial phase modulation of wavefronts in spatial filtering and holography, *J. Soc. Opt. Am.*, **56**(1966), 1167-1171

[59]   Hannes H., Interferometric measurements of phase structures in photographs, *J. Opt. Soc. Am.*, **58**(1968), 140-141

[60]   Brui E.B., Koreshev S.N., Charcteristics of use of thin layers of PE-2 photoemulsion for obtaining low frequency relief structures, *Opt. Spectrosc.* (USSR), **67**(1989), 403-405

[61]   Koreshev S.N., Gil S.V., Profile of low frequency relief hologram structures obtained on thin layers of PE-2 photoemulsion, *Opt. Spectrosc.* (USSR), **68**(1990), 247-249

[62]   Galpern A.D., Kalinina I.V., Selyavko L.V., Smaev V.P., Obtaining relief-phase holograms on PE-2 photographic plates and their copying, *Opt. Spectrosc.* (USSR), **60**(1986), 644-645

VITA

Fevzi Necati Ecevit was born in Beyşehir, Konya on April 18, 1962. He received his B.S. and M.S. degrees in Physics from the Middle East Technical University in June 1985 and in February 1988 respectively. He has been a Research Assistant in the Physics Department since 1985. His main areas of interest are holography and its application, computer programming, lasers and electronics.